Synthesis, structural and *in vitro* biological evaluation of diamondoid-decorated lipophilic organotin(IV) derivatives

Tushar S. Basu Baul,[a,*] Rajesh Manne,[a] Andrew Duthie,[b] Li Yuan Liew,[c,d] Jactty Chew,[d] See Mun Lee,[c] Edward R. T. Tiekink,[c,*]

[a]*Centre of Advanced Studies in Chemistry, North-Eastern Hill University, NEHU Permanent Campus, Umshing, Shillong 793 022, India*

[b]*School of Life and Environmental Science, Deakin University, Waurn Ponds, Victoria 3216, Australia*

[c]*Research Centre for Crystalline Materials, School of Medical and Life Sciences, Sunway University, 47500 Bandar Sunway, Selangor Darul Ehsan, Malaysia*

[d]*Department of Biological Sciences, School of Medical and Life Sciences, Sunway University, 47500 Bandar Sunway, Selangor Darul Ehsan, Malaysia*

ABSTRACT

A series of diamondoid-decorated organotin(IV) derivatives of composition $Me_3Sn(L^1)$ (**1**), $Ph_3Sn(L^1)$ (**2**), $\{[Me_2Sn(L^1)]_2O\}_2$ (**3**), $[BzSn(O)(L^1)]_6$ (**4**), $Me_3Sn(L^2)OH_2$ (**5**), $[Ph_3Sn(L^2)]_n$ (**6**), $Bu_2Sn(L^2)_2$ (**7**), $Bz_2Sn(L^2)_2OH_2$ (**8**) and $[BzSn(O)(L^2)]_6$ (**9**) were prepared by reacting appropriate organotin(IV) precursors with either acid forms of the pro-ligands adamantane-1-carboxylic acid (HL^1) and 2-(adamantan-1-yl)acetic acid (HL^2) or their sodium salts. Compounds **1**-**9** were characterised by spectroscopic techniques, including ^{119}Sn NMR in non-coordinating solvent for assessment of the solution-state structures. The molecular and crystal structures of **2**-**8** were established by X-ray crystallography. The packing is largely dictated by hydrophobic interactions with the exception in the crystals of **6**, where Sn···O secondary bonding is apparent, and in each of **5** and **8** where O–H···O hydrogen bonding is present leading to a two-dimensional array and zig-zag chains, respectively. The organotin compounds were evaluated for their anti-bacterial activity against 15 human bacterial pathogens. Based on disc diffusion and minimum inhibitory concentration assays, the two triphenyltin species, **2** and **6**, and di-n-butyl species, **7**, are effective against both Gram-positive and Gram-negative bacteria, including methicillin resistant *Staphylococcus aureus* (MTCC 381123) and *Shigella flexneri* (ATCC 12022), a causative agent for shigellosis. Time-kill assays showed that **2** and **6** had both time- and concentration-dependent anti-bacterial effects against susceptible bacteria. Cell viability assays showed that **2** and **6** were moderately toxic to a normal cell line, that is, human embryonic kidney 293T (HEK293T).

Keywords: Organotin/ Carboxylates/ Adamantly derivatives/ Hydrogen bonding/ Anti-bacterial properties/ Pharmacokinetics

*Corresponding authors.

E-mail addresses: basubaul@nehu.ac.in, basubaulchem@gmail.com (T. S. Basu Baul), edwardt@sunway.edu.my (Edward R. T. Tiekink).

1. Introduction

Adamantane (tricyclo-decane) is the smallest archetypal of diamondoid-hydrogen-terminated hydrocarbons with a diamond-like structure and its derivatives are compounds with high symmetry and striking impact [1-3]. The applications of adamantane derivatives in biology have grown at a rate comparable to the advancement of Amantadine (1-adamantylamine) chemistry. Amantadine became the forerunner of adamantane-based drug discovery due to its potent anti-Influenza A activity [4,5]. While Amantadine is no longer endorsed as an anti-Influenza A agent because of the development of resistance to this drug, it has been superseded by second-generation derivatives, such as Memantine (3,5-dimethyl-1-adamantanamine), with a total of seven adamantane-based drugs being approved for clinical use. However, these drugs were not discovered using modern high throughput screening strategies and their properties were typically determined on the basis of developing commercially available adamantane derivatives such as Amantadine or adamantane carboxylic acids. The adamantane moiety is widely incorporated in design and synthesis of new drugs in order to increase the stability and lipophilicity of molecules, thereby improving their pharmacokinetics [5-7]. The adamantyl moiety can be suitably tailored to fit the cavities of various host molecules such as cyclodextrins [8-10], can act as a blocking agent for cellular ion channels [11,12] and can also be integrated into the lipophilic part of the lipid bilayer so drug transfer can be made through cell membranes [13]. The value of the adamantyl group in drug design is multi-dimensional and its therapeutic aspects have been summarised [14].

While the adamantyl functionality has been widely utilised for anti-viral, anti-microbial and anti-cancer drugs [5,14], with recent attention focused on adamantane-based compounds for various biological applications [15-20], they are rarely used as ligands. Metal complexes of Pd(II), Pt(II), Cu(II) [21,22] and Ag [23] with admantane derivatives have

demonstrated anti-cancer and strong anti-microbial actions. Adamantane-based compounds are a multifaceted building block due to its rigid and precisely defined geometrical shape, steric demand and physical properties [24]. It can function as an anchoring unit for self-assembled monolayers, ensuring fixed angles of the adsorbed molecule relative to the metal surface [25]. Diamondoid-decorated Sn/S clusters were also accomplished by grafting adamantane units upon mono- and poly-functionalisation to bind Sn/S precursor clusters [26]. With the advent of a large variety of functionalisation on the adamantane core and the availability of even more lipophilic diamondoid building blocks discussed above, much is anticipated for the use of these unique hydrocarbons as modifiers or enhancers of active pharmacophores, an arena for future drug development. Complementing the above, research activities in the field of inorganic and organic chemistry of tin have advanced steadily due to their structural diversity and chemical applications, such as catalysis [27,28], antiproliferative activity [29], as well as biological applications [30-32]. A prominent element in anti-bacterial research is tin, usually present as an organometallic species, and a comprehensive review of the potential of these compounds as anti-bacterial agents has appeared [33]. In recent years, a broad range of synthetic organotin compounds have been investigated it his context including those of dithiocarbamates [34], hydroxamates [35], thiosemicarbazones [36] and, especially, carboxylates [37,38], sometimes derived from organic anti-bacterial agents, such as Ciprofloxacin [39]. The carboxylates chosen in the present study are derived from the symmetric cage compound adamantane, which is, as mentioned above, lipophilic in nature. While the anti-viral and anti-Parkinson effects of adamantane and derivatives are now well established [5] with a more recent development being the approval of an adamantane-1-carboxamide derivative (ABC294640), a sphingosuine kinase inhibitor, which is an anti-cancer drug used for the treatment of solid tumours [40].

With the above in mind, the current research deals with synthesis and characterisation

of organotin(IV) compounds with adamantane-1-carboxylate (L^1) and 2-(adamantan-1-yl)acetate (L^2) ligands (Scheme 1), which led to the isolation of various compounds of compositions $Me_3Sn(L^1)$ (**1**), $Ph_3Sn(L^1)$ (**2**), $\{[Me_2Sn(L^1)]_2O\}_2$ (**3**), $[BzSn(O)(L^1)]_6$ (**4**), $Me_3Sn(L^2)OH_2$ (**5**), $[Ph_3Sn(L^2)]_n$ (**6**), $Bu_2Sn(L^2)_2$ (**7**), $Bz_2Sn(L^2)_2OH_2$ (**8**) and $[BzSn(O)(L^2)]_6$ (**9**). Detailed structural information of compounds **1**-**9** in solution was obtained from multinuclear NMR spectroscopy, while single-crystal X-ray diffraction results provided information on the solid-state organisation of organotin(IV) compounds **2**-**8** in their crystals. In addition, the anti-bacterial activity of five of the new organotin compounds (**1**, **2**, **5**-**7**) was evaluated against 15 bacterial species using disc diffusion, MIC and MBC assays. Time-kill assays were conducted to determine the preliminary pharmacokinetics of the most active compounds, namely, **2** and **6**, were also conducted to assess the inhibition effects, i.e. bacteriostatic or bactericidal. Finally, the preliminary cytotoxicity effects of the compounds **2** and **6** were evaluated on a representative normal cell line, i.e. the human embryonic kidney epithelial cell line (HEK293T).

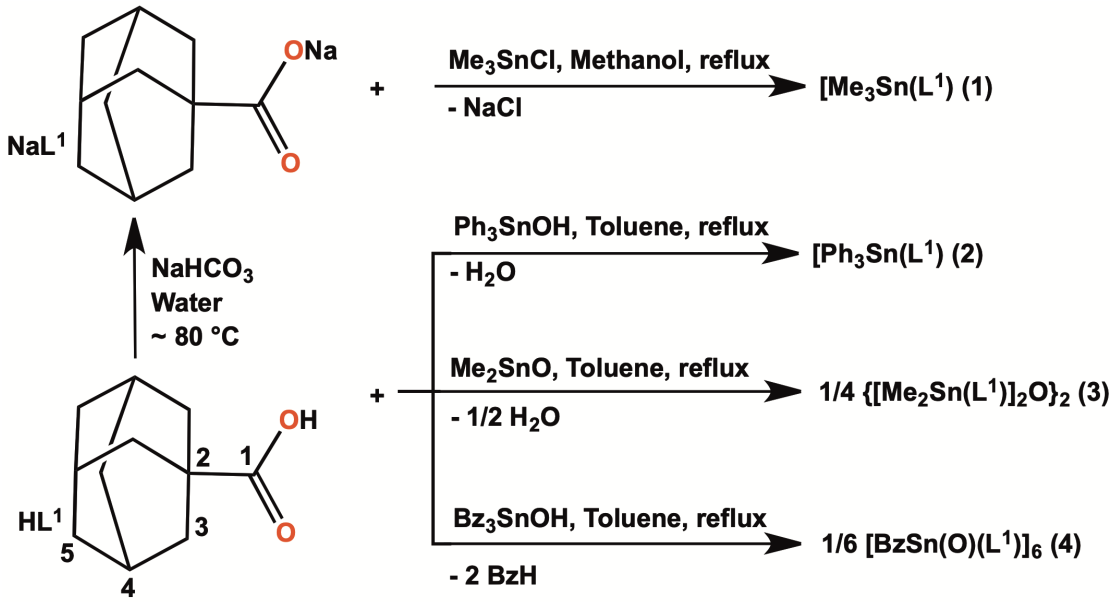

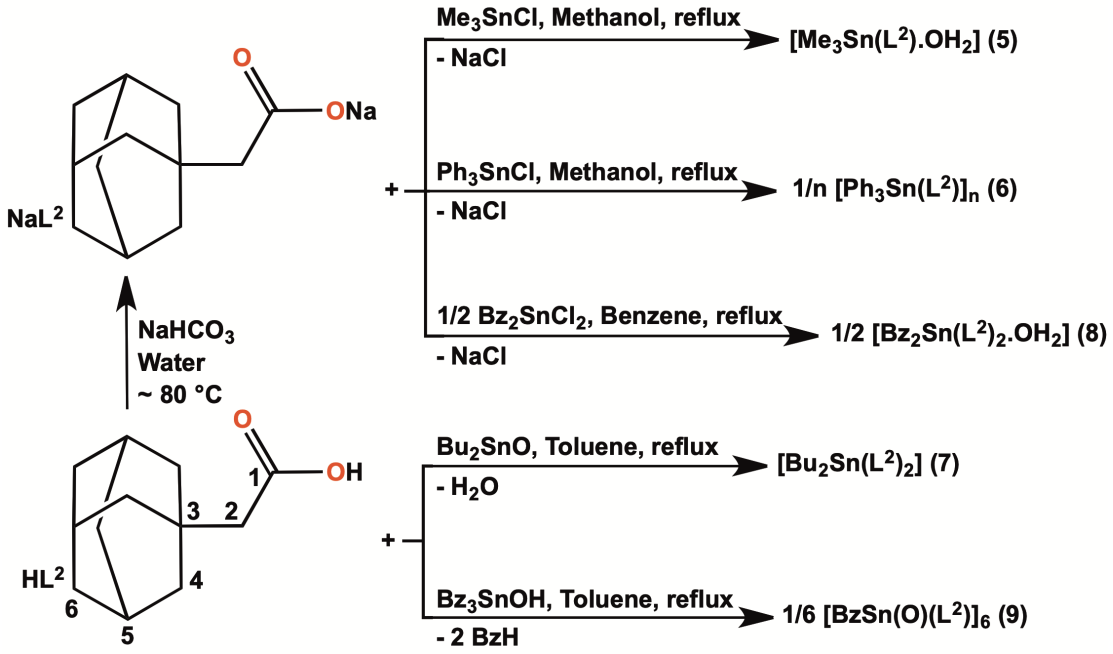

Scheme 1. Synthetic methodologies used for obtaining organotin(IV) compounds **1**-**9**. The numbers at the pro-ligands (HL^1 and HL^2) denote the atom-numbering protocol used for the NMR signal assignment.

2. Experimental

2.1. Materials and physical measurements

Solvents and other general reagents used in this work were purified according to standard procedures [41]. Adamantane-1-carboxylic acid, 2-(adamantan-1-yl)acetic acid, Me_2SnO, Me_3SnCl (Aldrich), Ph_3SnCl, Ph_3SnOH (Alfa Aesar) and Bu_2SnO (Merck) were used without further purification. Bz_3SnOH and Bz_2SnCl_2 were prepared according to literature procedures [42,43]. *Note*: The reaction for obtaining compound **8** can be conducted in toluene; however, synthetic convenience, particularly in response to the high boiling point of toluene, led to the choice of benzene. Care in handling benzene should be exercised. The same comment is valid for the other compounds wherever applicable.

Melting points were measured using a Büchi M-560 melting point apparatus and are uncorrected. Elemental analyses were performed using a Perkin Elmer 2400 series II

instrument. IR spectra in the range 4000-400 cm^{-1} were obtained either on a Perkin Elmer Spectrum BX series or Bruker alpha-II FT-IR spectrophotometer with samples investigated as KBr discs (ESI Figs. S1-S9). The ^{1}H and ^{13}C NMR spectra were recorded on a Bruker AMX 400 spectrometer and measured at 400.13 and 100.62 MHz, respectively (ESI Figs. S10-S27). ^{119}Sn NMR spectra were measured on a JEOL Zeta ECZ 400R spectrometer at 149.08 MHz (ESI Figs S28). The ^{1}H, ^{13}C and ^{119}Sn chemical shifts were referenced to Me_4Si (δ 0.00 ppm), $CDCl_3$ (δ 77.00 ppm) and Me_4Sn (δ 0.00 ppm), respectively.

2.2. Synthesis of the sodium salts

2.2.1. Sodium adamantane-1-carboxylate, Na(L^1)

A solution of sodium bicarbonate (0.46 g, 5.47 mmol) in hot water (5 mL) was added drop-wise to a suspension of HL^1 (0.50 g, 2.77 mmol) in hot water (10 mL) and digested for 1 h on a water bath. The resulting clear solution was filtered while hot. The filtrate was concentrated to dryness, treated with anhydrous methanol and finally dried *in vacuo*. The dried solid was extracted with anhydrous methanol with occasional warming on a water bath and filtered while hot. Evaporation of the filtrate afforded an amorphous, colourless powder, which was dried *in vacuo*. The solid was heated at reflux for 2 h in anhydrous toluene using a Dean-Stark apparatus to remove traces of moisture. Then, the solvent was removed on a rotary evaporator and the product dried *in vacuo*. Yield (0.51 g, 90%), M.p.: >350 °C. IR absorptions (cm^{-1}): 3630, 3397, 2908, 2848, 1655 $\nu(OCO)_{asym}$, 1623, 1527, 1452, 1410, 1343, 1315, 1260, 1180, 1104, 906, 799, 766, 683, 608.

2.2.2. Sodium 2-(adamantan-1-yl)acetate, Na(L^2)

An analogous method to that used for the preparation of Na(L^1) was followed, using 2-(adamantan-1-yl)acetic acid. The product was recrystallised from anhydrous methanol, giving

a colourless powder of Na(L^2) in 50% yield. M.p.: >350 °C. IR absorption (cm^{-1}): 3421, 2094, 2847, 1631 $\nu(OCO)_{asym}$, 1575, 1556, 1440, 1408, 1344, 1313, 1146, 1101, 797, 663.

2.3. Synthesis of organotin(IV) compounds 1-9

2.3.1. Synthesis of $Me_3Sn(L^1)$ (1)

Me_3SnCl (0.50 g, 2.50 mmol) in methanol (20 mL) was added to a clear solution of NaL^1 (0.51 g, 2.50 mmol) in methanol (30 mL) with continuous stirring. The reaction mixture was then refluxed for 5 h and filtered while hot to remove NaCl. The filtrate was evaporated using a rotary evaporator; the residue washed twice with hexane (2 × 0.5 mL) and dried *in vacuo*. The residue was extracted into toluene and filtered to remove any suspended particles. The slow evaporation of the filtrate at room temperature for several days afforded colourless crystals of **1**. Yield 0.61 g (70%), M.p.: 190-192 °C. Anal. found. C, 48.88; H, 6.78. Calcd. for $C_{14}H_{24}O_2Sn$: C, 49.02; H, 7.05%. IR absorptions (cm^{-1}): 3433, 2904, 2851, 1591 $\nu(OCO)_{asym}$, 1450, 1374, 1363, 1306, 1189, 1110, 1088, 779, 764, 679, 554, 546. ^{1}H NMR ($CDCl_3$) δ_H (ppm): 1.99 [s, 3H, H-4], 1.87 [s, 6H, H-3], 1.70 [s, 6H, H-5], 0.50 [s, 9H, H-1*] [$^2J(^1H\text{-}^{119}Sn)$ = 60 Hz]. ^{13}C NMR ($CDCl_3$) δ_C (ppm): 183.80 [C-1], 40.62 [C-2], 39.41 [C-3], 36.60 [C-5], 28.14 [C-4], –2.48 [$^1J(^{13}C\text{-}^{119}Sn)$ = 399 Hz, C-1*]. ^{119}Sn NMR ($CDCl_3$): δ_{Sn} (ppm): 125.0.

2.3.2. Synthesis of $Ph_3Sn(L^1)$ (2)

Ph_3SnOH (0.50 g, 1.38 mmol) in toluene (50 mL) was added to a clear solution of HL^1 (0.25 g, 1.38 mmol) in toluene (15 mL). The reaction mixture was heated at reflux for 5 h using a Dean-Stark apparatus and a water-cooled condenser, filtered while hot and the filtrate evaporated to dryness. The residue was washed with anhydrous hexane (2 × 0.5 mL) and dried *in vacuo*. The residue was extracted into toluene and filtered to remove any suspended

particles. Slow evaporation of the filtrate at room temperature yielded microcrystalline material. Several recrystallisation cycles from toluene afforded colourless crystals of **2**. Yield: 0.50 g (68%). M.p.: 140-142 °C. Anal. found. C, 65.58; H, 5.48. Calcd. for $C_{29}H_{30}O_2Sn$: C, 65.81; H, 5.71%. IR absorptions (cm^{-1}): 3066, 2905, 2846, 1624 $\nu(OCO)_{asym}$, 1480, 1451, 1430, 1342, 1297, 1255, 1180, 1105, 1079, 806, 728, 698, 684, 575. ^1H NMR ($CDCl_3$) δ_H (ppm): 7.78-7.63 [m, 6H, H-2*], 7.43 [m, 9H, H-3*/H-4*], 1.99 [s, 3H, H-4], 1.94 [s, 6H, H-3], 1.70 [s, 6H, H-5]. ^{13}C NMR ($CDCl_3$) δ_C (ppm): 184.87 [C-1], 138.76 [$^1J(^{13}C\text{-}^{119}Sn)$ = 645 Hz, C-1*], 136.78 [$^2J(^{13}C\text{-}^{119}Sn)$ = 48 Hz, C-2*], 129.90 [$^4J(^{13}C\text{-}^{119}Sn)$ = 10 Hz, C-4*], 128.77 [$^3J(^{13}C\text{-}^{119}Sn)$ = 63 Hz, C-3*], 40.58 [C-2], 39.39 [C-3], 36.51 [C-5], 28.07 [C-4]. ^{119}Sn NMR ($CDCl_3$) δ_{Sn} (ppm): –118.7.

2.3.3. Synthesis of $\{[Me_2Sn(L^1)]_2O\}_2$ (3)

A suspension of Me_2SnO (0.20 g, 1.21 mmol) and HL^1 (0.21 g, 1.21 mmol) in anhydrous toluene (40 mL) was refluxed for 5 h in a flask equipped with a Dean-Stark water separator and a water-cooled condenser. The clear reaction mixture was filtered while hot and the filtrate evaporated to dryness. The residue was washed with anhydrous hexane (3 × 1 mL) and dried *in vacuo*. The residue was extracted in boiling benzene and filtered while hot. The slow evaporation of the filtrate furnished colourless crystals of **3**. Yield: 0.25 g (81%). M.p.: 277-279 °C. Anal. found. C, 46.28; H, 6.66. Calcd. for $C_{52}H_{84}O_{10}Sn_4$: C, 46.47; H, 6.30%. IR absorptions (cm^{-1}): 3450, 2905, 2849, 1634 $\nu(OCO)_{asym}$, 1546, 1452, 1416, 1332, 1313, 1291, 1250, 791, 787, 654, 521, 504, 480. ^1H NMR ($CDCl_3$) δ_H (ppm): 1.99 [s, 3H, H-4], 1.80 [s, 6H, H-3], 1.69 [m, 6H, H-5], 0.79 and 0.70 [s, 6H H-1*]. ^{13}C NMR ($CDCl_3$) δ_C (ppm): 184.86 [C-1], 41.15 [C-2], 39.43 [C-3], 36.63 [C-5], 28.16 [C-4], 9.66 and 6.85 [C-1*]. ^{119}Sn NMR ($CDCl_3$) δ_{Sn} (ppm): –190.0 and –193.4.

2.3.4. Synthesis of $[BzSn(O)(L^1)]_6$ (4)

An analogous method to that used for the preparation of **3** was followed using Bz_3SnOH (0.20 g, 0.48 mmol) and HL^1 (0.09 g, 0.48 mmol). The product was crystallised from a large volume of anhydrous toluene, giving colourless crystals of **4** upon slow evaporation. Yield: 0.15 g (75%). M.p.: 340-342 °C. Anal. found. C, 53.28; H, 5.08. Calcd. for $C_{108}H_{132}O_{18}Sn_6$: C, 53.37; H, 5.47%. IR absorptions (cm^{-1}): 2904, 2849, 1573 $\nu(OCO)_{asym}$, 1524, 1493, 1452, 1427, 1312, 1113, 755, 693, 627, 592, 496. ^1H NMR ($CDCl_3$) δ_H (ppm): 7.27 [t, 2H, H-3*], 7.17 [t, 2H, H-4*], 7.02 [t, 1H, H-5*], 2.70 [s, $^2J(^1H\text{-}^{119}Sn)$ = 148 Hz, 2H, H-1*], 1.90 [s, 3H, H-4], 1.67-1.53 [m, 12H, H-3/H-5]. ^{13}C NMR ($CDCl_3$) δ_C (ppm): 185.04 [C-1], 139.33 [C-2*], 129.23 [C-4*], 127.81 [C-3*], 124.05 [C-5*], 42.43 [C-2], 38.60 [C-3], 36.61 [C-5], 34.34 [C-1*], 28.12 [C-4]. ^{119}Sn NMR ($CDCl_3$) δ_{Sn} (ppm): –520.6.

2.3.5. Synthesis of $Me_3Sn(L^2)OH_2$ (5)

An analogous method to that used for the preparation of **1** was followed using Me_3SnCl (0.50 g, 2.50 mmol) and NaL^2 (0.55 g, 2.57 mmol). The product was crystallised from ethanol, giving colourless crystals of **5** upon slow evaporation. Yield: 0.75 g (81%). M.p.: 180-182 °C. Anal. found. C, 48.08; H, 7.48. Calcd. for $C_{15}H_{28}O_3Sn$: C, 48.03; H, 7.52%. IR absorptions (cm^{-1}): 2925, 2900, 1605 $\nu(OCO)_{asym}$, 1442, 1377, 1358, 1344, 1297, 1192, 1148, 1100, 783, 720, 677, 558, 549. ^1H NMR ($CDCl_3$) δ_H (ppm): 4.71 [s, 2H, H_2O], 2.01 [s, 2H, H-2], 1.89 [s, 3H, H-5], 1.64-1.55 [m, 12H, H-4/H-6], 0.47 [s, $^2J(^1H\text{-}^{119}Sn)$ = 56 Hz, 9H, H-1*]. ^{13}C NMR ($CDCl_3$) δ_C (ppm): 177.66 [C-1], 49.52 [C-2], 42.43 [C-4], 36.82 [C-6], 32.41 [C-3], 28.64 [C-5], –2.41 [$^1J(^{13}C\text{-}^{119}Sn)$ = 399 Hz, C-1*]. ^{119}Sn NMR ($CDCl_3$) δ_{Sn} (ppm): 125.6.

2.3.6. Synthesis of $[Ph_3Sn(L^2)]_n$ (6)

An analogous method to that used for the preparation of **1** was followed using Ph_3SnCl (0.50 g, 1.29 mmol) and NaL^2 (0.30 g, 1.38 mmol). The product was crystallised from ethanol, giving colourless crystals of **6** upon slow evaporation. Yield: 0.55 g (78%). M.p.: 138-140 °C. Anal. found. C, 66.78; H, 6.08. Calcd. for $C_{30}H_{32}O_2Sn$: C, 66.32; H, 5.94%. IR absorptions (cm^{-1}): 3063, 3048, 2905, 2848, 1574 $\nu(OCO)_{asym}$, 1543, 1519, 1482, 1429, 1418, 1403,1311, 1080, 728, 698. ^1H NMR ($CDCl_3$) δ_H (ppm): 7.82 [m, 6H, H-2*], 7.51 [m, 9H, H-3*/H4*], 2.25 [s, 2H, H-2], 1.95 [s, 3H, H-5], 1.72-1.57 [m, 12H, H-4/H-6]. ^{13}C NMR ($CDCl_3$) δ_C (ppm): 179.29 [C1], 138.65 [$^1J(^{13}C\text{-}^{119}Sn)$ = 649 Hz, C-1*], 136.90 [$^2J(^{13}C\text{-}^{119}Sn)$ = 48 Hz, C-2*], 129.96 [$^4J(^{13}C\text{-}^{119}Sn)$ = 13 Hz, C-4*], 128.76 [$^3J(^{13}C\text{-}^{119}Sn)$ = 62 Hz, C-3*], 48.72 [C-2], 42.37 [C-4], 36.67 [C-6], 32.81 [C-3], 28.58 [C-5]. ^{119}Sn NMR ($CDCl_3$) δ_{Sn} (ppm): –117.7.

2.3.7. Synthesis of $Bu_2Sn(L^2)_2$ (7)

An analogous method to that used for the preparation of **2** was followed using Bu_2SnO (0.25 g, 1.00 mmol) and HL^2 (0.39 g, 2.00 mmol). The product was crystallised from ethanol, giving colourless crystals of **7** upon slow evaporation. Yield: 0.45 g (72%). M.p.: 72-74 °C. Anal. found. C, 62.28; H, 7.98. Calcd. for $C_{32}H_{52}O_4Sn$: C, 62.04; H, 8.46%. IR absorptions (cm^{-1}): IR absorptions (cm^{-1}): 2952, 2905, 2847, 1589 $\nu(OCO)_{asym}$, 1451, 1378, 1147, 1125, 727, 674. ^1H NMR ($CDCl_3$) δ_H (ppm): 2.07 [s, 2H, H-2], 1.91 [s, 3H, H-5], 1.65-1.29 [m, 16H, H-4/H-6/H-1*/H-2*], 1.34-1.29 [m, 2H, H-3*], 0.84 [t, 3H, H-4*]. ^{13}C NMR ($CDCl_3$) δ_C (ppm): 182.45 [C-1], 48.69 [C-2], 42.44 [C-4], 36.71 [C-6], 32.58 [C-3], 28.57 [C-5], 26.79 [C-2*], 26.41 [C-3*], 25.16 [$^1J(^{13}C\text{-}^{119}Sn)$ = 591 Hz, C-1*], 13.52 [C-4*]. ^{119}Sn NMR ($CDCl_3$) δ_{Sn} (ppm): –150.0.

2.3.8. Synthesis of $Bz_2Sn(L^2)_2OH_2$ (8)

An analogous method to that used for the preparation of **1** was followed using Bz_2SnCl_2 (0.25 g, 0.67 mmol) and NaL^2 (0.29 g, 1.34 mmol). The product was crystallised from ethanol, giving colourless crystals of **8** upon slow evaporation. Yield: 0.35 g (73%). M.p.: 110-112 °C. Anal. found. C, 64.98; H, 7.40. Calcd. for $C_{38}H_{50}O_5Sn$: C, 64.69; H, 7.14%. IR absorptions (cm^{-1}): 2908, 2847, 1653, 1585 $\nu(OCO)_{asym}$, 1543, 1492, 1452, 1432, 1409, 1147, 1104, 1050, 766, 754, 696, 671, 620. ^1H NMR ($CDCl_3$) δ_H (ppm): 7.11-7.00 [m, 10H, H-3*/H-4*/H-5*], 4.53 [s, 2H, H_2O], 2.88 [s, $^2J(^1H\text{-}^{119}Sn)$ = 100 Hz, 2H, H-1*], 1.87-1.85 [m, 10H, H-2/H-5], 1.63-1.52 [m, 12H, H-4], 1.50 [s, 12H, H-6]. ^{13}C NMR ($CDCl_3$) δ_C (ppm): 181.48 [C-1], 136.50 [C-2*], 128.31 [C-4*], 127.94 [C-3*], 124.80 [C-5*], 47.86 [C-2], 41.98 [C-4], 36.36 [C-6], 33.57 [C-3], 32.06 [C-1*], 28.18 [C-5]. ^{119}Sn NMR ($CDCl_3$) δ_{Sn} (ppm): –244.8.

2.3.9. Synthesis of $[BzSn(O)(L^2)]_6$ (9)

An analogous method to that used for the preparation of **3** was followed using Bz_3SnOH (0.30 g, 0.73 mmol) and HL^2 (0.14 g, 0.73 mmol). The product crystallised as a fine, colourless microcrystalline material from a large volume of hot anhydrous toluene when heated at water-bath temperature. Yield: 0.25 g (81%). M.p.: 278-279 °C. Anal. found. C, 54.28; H, 6.18. Calcd. for $C_{114}H_{144}O_{18}Sn_6$: C, 54.45; H, 5.77%. IR absorptions (cm^{-1}): 2900, 2847, 1586 $\nu(OCO)_{asym}$, 1536, 1449, 1413, 1362, 1346, 1308, 1151, 1097, 1077, 991, 728, 696, 621, 553, 524. ^1H NMR ($CDCl_3$) δ_H (ppm): 7.11-7.00 [m, 5H, H-3*/H-4*/H-5*], 2.88 [s, $^2J(^1H\text{-}^{119}Sn)$ = 100 Hz, 2H, H-1*], 1.85 [m, 5H, H-2/H-5], 1.60-1.50 [m, 12H, H-4/H-6]. ^{13}C NMR ($CDCl_3$) δ_C (ppm): 181.48 [C-1], 136.52 [C-2*], 128.31 [C-4*], 127.92 [C-3*], 124.78 [C-5*], 47.91 [C-2], 41.97 [C-4], 36.35 [C-6], 33.62 [C-3], 32.05 [C-1*], 28.17 [C-5]. ^{119}Sn NMR ($CDCl_3$) δ_{Sn} (ppm): –520.7.

(Note: Numbers 1*, 2*, 3*, 4* and 5* refer to the proton and carbon atoms of the Sn-R moiety).

2.4. Single crystal X-ray structure determination

Crystal data and refinement details for **2**-**8** are included in Table 1. Intensity data for the colourless crystals were measured at room temperature on an Agilent Xcalibur Eos Gemini diffractometer equipped with a CCD area detector and graphite-monochromated Mo Kα radiation (λ = 0.71073 Å). Data reduction and empirical absorption corrections, based on a multi-scan technique, were applied [44]. The structures were solved by direct methods [45] and refined on F^2 with anisotropic displacement parameters and C-bound H atoms in the riding model approximation [46]. For **5** and **8**, the oxygen-bound H atoms were refined with a distance restraint O–H = 0.82±0.01 Å. A weighting scheme of the form $w = 1/[\sigma^2(F_o^2) + (aP)^2 + bP]$ where $P = (F_o^2 + 2F_c^2)/3)$ was introduced for each refinement. For **5**, the maximum and minimum residual electron density peaks of 1.05 and 1.70 eÅ^{-3}, respectively, were located 1.83 and 1.39 Å from the H2o and H15a atoms, respectively, i.e. in chemically non-relevant positions. The molecular structure diagrams were generated by ORTEP for Windows [47] and the packing diagrams with DIAMOND [48]. Additional data analysis was made with PLATON [49].

Insert Table 1

2.5. Screening for anti-bacterial activity

2.5.1. Bacterial species

Fifteen clinically relevant bacterial species were used in this study, purchased from either the American Type Culture Collection (ATCC) or the Malaysian Type Culture Collection (MTCC). Six of these pathogens were Gram-positive bacteria: *Enterococcus faecalis* (ATCC

33186), *Enterococcus faecium* (ATCC 19434), Methicillin Resistant *Staphylococcus aureus* (MRSA; MTCC 381123), *Staphylococcus epidermidis* (ATCC 700576), *Streptococcus pneumoniae* (ATCC 49619) and *Streptococcus pyogenes* (ATCC 49399). The nine Gram-negative bacteria were *Escherichia coli* (ATCC 11775), *Escherichia coli* clinical isolate K1 (MTCC 710859), *Klebsiella pneumoniae* (ATCC 13883), *Klebsiella quasipneumoniae* (ATCC 700603), *Pseudomonas aeruginosa* (ATCC 10145), *Proteus vulgaris* (ATCC 49990), *Salmonella enterica* (ATCC 14028), *Shigella flexneri* (ATCC 12022) and *Vibrio parahaemolyticus* (ATCC 17802). The bacterial cultures were maintained on nutrient agar (Oxoid) and sub-cultured on a weekly basis. Prior to all experiments, the bacteria were cultured in Mueller-Hinton Broth (MHB; Oxoid) and incubated overnight at 37 °C.

2.5.2. Disc diffusion assay

The anti-bacterial activities of the trial compounds were screened using a conventional disc diffusion method in accordance with the Clinical and Laboratory Standards Institute (CLSI) guidelines. An inoculum suspension of each bacterial species was prepared by diluting the turbidity of overnight-grown cultures to OD_{625} nm = 0.09-0.13, equivalent to 1-2 x 10^8 colony forming units (CFU)/mL, using phosphate buffer saline (PBS; Sigma-Aldrich). The adjusted inoculum suspension was then spread on Mueller-Hinton agar (MHA; Oxoid) using a sterile cotton swab. Sterile filter paper discs (6 mm in diameter) were aseptically placed on the agar followed by the addition of 5 µL of each trial compound with a stock concentration of 6 mg/mL, resulting in discs containing 30 µg of compound. Two anti-biotics, tetracycline (30 µg/disc) and chloramphenicol (30 µg/disc), were included in the experiments as positive controls while discs containing 5 µL of each DMSO and broth medium were included as solvent and negative controls, respectively. The plates containing the discs were incubated at 37 °C for 24 h. The anti-bacterial activities of the trial compounds were determined by

measuring the diameter of inhibition zones formed around the discs. Three independent experiments were conducted for each compound.

2.5.3. Minimum inhibitory concentration (MIC) and Minimum bactericidal concentration (MBC) assays

Following disc diffusion screening, the determination of the anti-bacterial activity of selected active compounds was tested using the broth dilution method to determine MIC and MBC values. The broth-dilution method was conducted according to CLSI protocols. Each test compound was taken up in DMSO to a concentration of 2 mg/mL, followed by a 2-fold dilution with DMSO. Graded concentrations of the trial compounds (5 µl) were added into each well of 96-well microplates, achieving final concentrations ranging from 0.78 to 100 µg/mL. The controls included in the assay were anti-biotics (Tetracycline and Chloramphenicol), DMSO (solvent) and broth medium (negative). After the addition of compounds and controls, inoculum suspension was added to wells, achieving 10^5 CFU/mL of cells in each well. Media with no bacterial suspension were also included as an additional negative control in the assay. The microplates were incubated for 24 h at 37 °C. The presence of turbidity observed in each well indicated bacterial growth. The MIC was determined as the lowest concentration at which no turbidity was seen. The suspension in each well was separately aliquoted and transferred onto MHA. After a 24 h incubation at 37 °C, the MBC was determined as the minimum concentration of a compound where no viable colony count was observed.

2.5.4. Time-kill assay

The anti-bacterial activities of two selected compounds, i.e. **2** and **6**, over time were evaluated using a time-kill assay. The inoculum suspension with a bacterial density of 10^5

CFU/mL was used in this assay. Each test compound (100 µL) was added to the inoculum suspension, giving a final volume of 10 mL and achieving final concentrations of ½ × MIC, 1 × MIC and 2 × MIC (MIC values were as determined in section 2.5.3). A growth control comprising only bacterial species was included in each replicate. All treated and untreated cultures were incubated at 37 °C on an orbital shaker operating at 200 r.p.m. The cultures were removed from shaker at each time interval of incubation (0, 1, 2, 4, 8 and 24 h). A total of 300 µL of suspension, each aliquot being100 µL, was removed from the cultures and each 10-fold titrated in 0.9% normal saline. Next, 10 µL of each dilution was then plated on MHA. All plates were incubated at 37 °C overnight. The experiments were performed in triplicate. The data were analysed as killing curves by plotting the $\log_{10}$[colony forming unit per millilitre (CFU/mL)] versus time (h). The viable bacterial cell counts for the time-kill end point determination, i.e. bactericidal activity, was defined as a reduction of $\geq 3\log_{10}$ (CFU/mL) relative to the initial inoculum, whereas the bacteriostatic activity corresponds to $< 3\log_{10}$ (CFU/mL) reduction relative to the initial inoculum.

2.5.5. Cell viability assay

The cytotoxicity of the trial compounds against human embryonic kidney cell line, HEK293T (ATCC CRL-3216) was studied using an MTT proliferation assay. The HEK293T cells were seeded in each well of a 96-well micro plate at a cell density of 2×10^4 cells/mL. Each test compound was dissolved and further 2-fold serial-diluted in DMSO. The pre-seeded HEK293T cells were treated with the compounds (pro-ligands: HL^1, HL^2, organotin compounds: **1**, **2**, **5**-**7**, organotin precursors: Me_3SnCl, Ph_3SnOH, Bu_2SnCl_2) at final concentrations ranging from 0.78 to 100 µg/mL with 1% (v/v) DMSO. Treatment lasted for 24 h at 37 °C. 10 µL of MTT (Goldbio) solution was added to each well. The plate was incubated for a further 4 h. The medium was removed from each well and replaced with

DMSO to dissolve insoluble formazan formed in the wells. The absorbance was measured at 540 nm through microplate reader (Tecan Infinite-M200). The 50% cytotoxic concentration (CC_{50}) of each trial compound was determined by plotting cell viability in the presence of different concentrations of the trial compounds. The results are the average of three independent experiments.

3. Results and discussion

3.1. Synthesis and characterisation of 1-9

The reactions of R_3SnCl (R = methyl or phenyl) with sodium adamantane-1-carboxylate, $Na(L^1)$ and sodium 2-(adamantan-1-yl)acetate, $Na(L^2)$ in methanol affords $Me_3Sn(L^1)$ (**1**), $Me_3Sn(L^2)OH_2$ (**5**) and $[Ph_3Sn(L^2)]_n$ (**6**). On the other hand, the reactions of Bz_3SnOH with adamantane-1-carboxylic acid (HL^1) and 2-(adamantan-1-yl)acetic acid (HL^2) in toluene at reflux temperature undergoes a facile double Sn-C bond cleavage to give the monoorganostannoxanes $[BzSn(O)(L^1)]_6$ (**4**) and $[BzSn(O)(L^2)]_6$ (**9**), respectively. In contrast, the reaction of Ph_3SnOH with HL^1 affords $Ph_3Sn(L^1)$ (**2**), where the Sn-C bonds are found to be robust. Diorganotin(IV) compounds of compositions $\{[Me_2Sn(L^1)]_2O\}_2$ (**3**) and $Bu_2Sn(L^2)_2$ (**7**) were obtained from reactions of the corresponding R_2SnO (R = methyl or butyl) with the appropriate HL^1/HL^2, while $Bz_2Sn(L^2)_2OH_2$ (**8**) was obtained by metathesis reaction of Bz_2SnCl_2 with $Na(L^2)$. The synthetic details are given in the Experimental Section (see also Scheme 1). The organotin(IV) compounds have been characterised by IR, ^1H, ^{13}C and ^{119}Sn NMR spectroscopic techniques. The FT-IR spectra of compounds **1-9** show a characteristic band for the $\nu_{asym}(OCO)$ vibration, which is significantly shifted (refer to the IR data for specific shift assignments and ESI Figs 1-9 for complete spectra of compounds) from their relative positions in pro-ligands HL^1 ($\nu_{asym}(OCO)$ = 1693 cm^{-1}) and HL^2 ($\nu_{asym}(OCO)$ = 1710 cm^{-1}), indicating coordination of the carboxylate group to the organotin fragments [50]. In addition, a characteristic medium to strong intensity band was

detected for compound **3** at ~ 655 cm^{-1} and for **4** and **9** at ~ 625 cm^{-1} that is assigned to the ν(Sn-O-Sn) vibration [51,52]. Compounds **1**-**9** display the anticipated ^{1}H and ^{13}C NMR signals in solution, revealing the general spectral patterns (ESI Figs S10-S27). The absence of the carboxylic/acetic acid OH proton signals of HL^1 and HL^2 in the compounds **1**-**9** supports the binding to the tin centre. For the ligand and Sn-R moieties, the number of protons calculated from the integration values in the ^{1}H NMR spectra agree with the proposed molecular structures of **1**-**9** (see Experimental Section). Compound **3** displayed two sets of ^{1}H and ^{13}C signals for the methyl groups, which is in accord with the pairwise heterotopic non-equivalence of the exocyclic and endocyclic Me_2Sn moieties. The solution structures of compounds **1**-**9** were determined by ^{119}Sn NMR chemical shifts in $CDCl_3$ and are collated in ESI Figs S28. Trimethyltin(IV) compounds **1** and **5** exhibit ^{119}Sn NMR chemical shifts at around +125 ppm, which is indicative of four-coordinated tin atoms [53]. The triphenyltin(IV) compounds **2** and **6** exhibited a single sharp resonance at higher fields at around −118 ppm, similar to other four-coordinated triphenyltin carboxylates [54]. Thus, from the δ (^{119}Sn) NMR values it may be inferred that the five-coordinate geometries of the tin atoms in the solid-state structures of **1**, **5** and **6** (either due to coordination of a water molecule or bidentate bridging) are not retained in solution (see Experimental Section). The ^{119}Sn NMR spectrum of the tetranuclear dimethyltin(IV) compound $\{[Me_2Sn(L^1)]_2O\}_2$ (**3**) with a bis(dicarboxylatotetraorganodistannoxane) framework displays a pair of resonances at around –190 and –193 ppm, confirming the presence of *endo*- and *exo*-cyclic tin atoms [51,52]. The δ (^{119}Sn) chemical shifts in the ranges –200 to –400, –90 to –190 and +200 to –60 ppm, respectively, have been associated with six-, five- and four-coordinate tin centres bearing alkyl groups [55]. On this basis, the two chemically different tin atom centres, i.e. *endo*-Sn and *exo*-Sn, are assigned to be five-coordinate and the results are consistent with those revealed by X-ray crystallography (*vide infra*). This signifies that the coordination environments of the tin atoms are robust and retained in non-coordinating $CDCl_3$ solution. The diorganotin(IV)

compounds of composition $Bu_2Sn(L^2)_2$ (**7**) and $Bz_2Sn(L^2)_2OH_2$ (**8**) necessitate specific mention. The ^{119}Sn NMR spectrum of **7** reveals a sharp signal at –150 ppm, consistent with those reported for other $Bu_2Sn(O_2CR')_2$ systems [56], implying that the same coordination pattern i.e. a trapezoidal-bipyramid as observed in the solid-state is preserved in solution. Compound **8** adopts a pentagonal-bipyramidal geometry in the solid-state (*vide infra*) and has a ^{119}Sn NMR signal at around –245 ppm in $CDCl_3$ solution. The observed chemical shift matches closely with five-coordinated dibenzyltin(IV) Schiff base aminoacetate [57], but the observed chemical shift value is much lower than the value observed for structurally characterised six-coordinate dibenzyltin(IV) oxinates [58], and hence a conclusion about the coordination in solution could not be derived unambiguously. Lastly, the ^{119}Sn NMR spectra of the monoorganostannoxanes **4** and **9** each exhibited single sharp resonance at *ca* – 520 ppm, indicative of the equivalence of the six tin atoms in the molecules of $[BzSn(O)(L^{1/2})]_6$, and this is corroborated by the observed drum structural motif [59,60].

3.2. Molecular structures of 2-8

The crystal and molecular structures of three organotin(IV) derivatives of HL^1, **2**-**4** (Fig. 1), and four organotin(IV) derivatives of HL^2, **5**-**8** (Fig. 2), have been established by X-ray crystallography. The molecule in $Ph_3Sn(L^1)$, **2**, is illustrated in Fig. 1a and features an asymmetrically chelating carboxylate ligand with the Sn–O1 and Sn–O2 bond lengths being 2.046(2) and 2.720(3) Å, respectively. The difference in the long and short Sn–O bond lengths amounts to approximately 0.67 Å and this is clearly reflected in the significant disparity in the associated C1–O1 and C1–O2 bond lengths of 1.295(4) and 1.220(4) Å, respectively. If the carboxylate ligand was considered monodentate, the C_3O donor set would define a tetrahedral geometry with the range of tetrahedral angles being a narrow at 94.89(9)°, for O1–Sn–C18, to a wide 118.43(9)°, for O1–Sn–C12, with the widest angle

clearly correlated with the close approach of the O2 atom to tin. If the Sn···O2 interaction was considered binding, the C_3O_2 donor set exhibits a far greater range of angles, being an acute 52.31(9)°, for the O1–Sn–O2 chelate angle, to 146.14(8)°, for O2–Sn–C18. The parameter, τ, can be employed to measure the deviation of a five-coordinate geometry from the ideal square pyramidal, for which τ = 0.00, and trigonal bipyramidal (τ = 1.00) geometries [61]. For **2**, τ computes to 0.46, i.e. almost perfectly intermediate between the extremes.

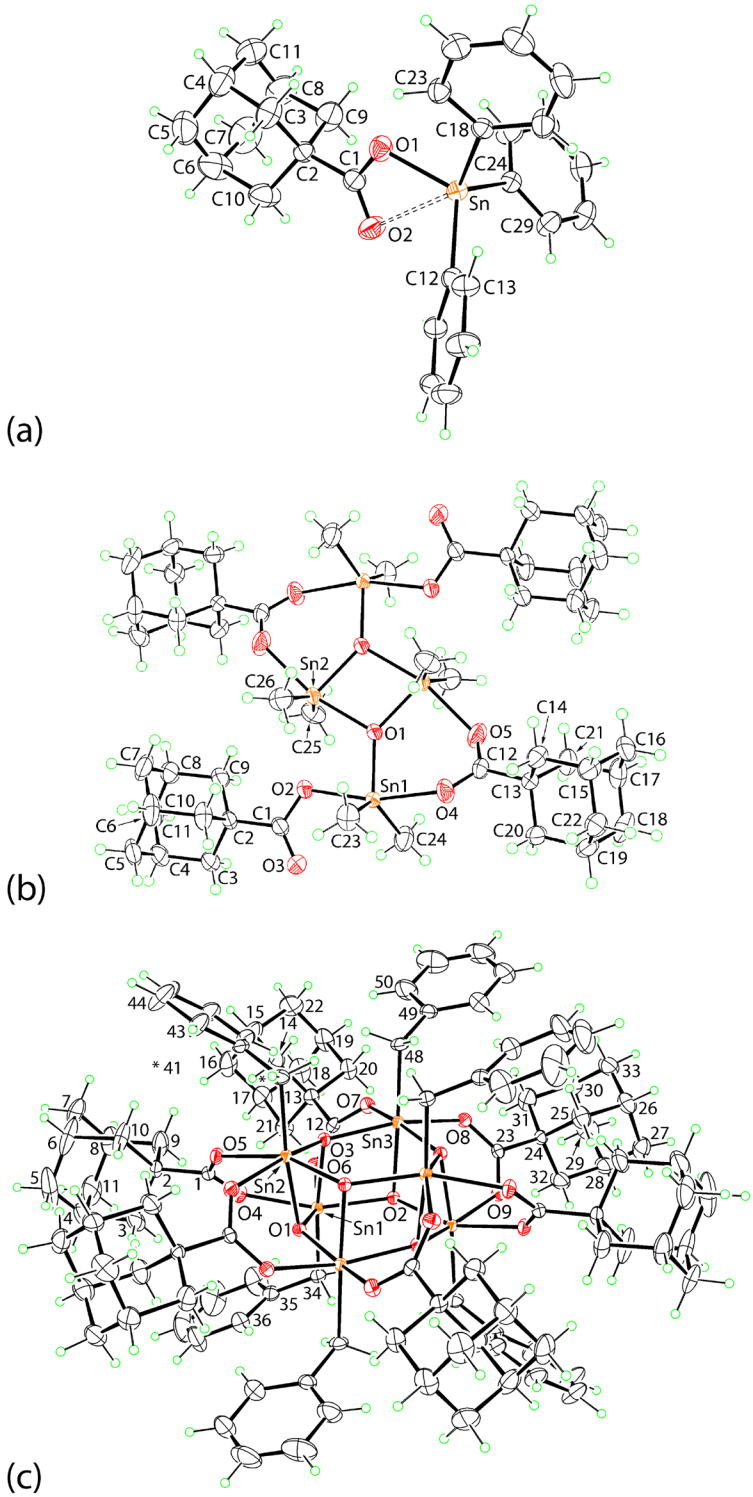

Fig. 1. The molecular structures of (a) $Ph_3Sn(L^1)$ (**2**; 25% probability level), (b) $\{[Me_2Sn(L^1)]_2O\}_2$ (**3**; 50% probability level) and (c) $[BzSn(O)(L^1)]_6$ (**4**; 25% probability level), showing the atom labelling schemes and anisotropic displacement parameters. The unlabelled atoms are related by the symmetry operation 2-x, 2-y, 2-z (**3**) and 2-x, 1-y, -z (**4**).

In **3**, the carbon atoms are indicated by numbers only to reduce cluttering. Selected geometric parameters for the bridging carboxylate ligands in **3**: Sn1–O4 = 2.141(3), Sn2–O5 = 2.140(3), C1–O4 = 1.260(5), C1–O5 = 1.252(5), Sn1–O6 = 2.167(3), Sn3–O7 = 2.139(3), C12–O6 = 1.257(5), C12–O7 = 1.266(5), Sn3–O8 = 2.140(3), Sn2–O9^{i} = 2.138(3), C23–O8 = 1.264(5), C23–O9 = 1.259(4) Å.

The molecular structure of tetra-nuclear $\{[Me_2Sn(L^1)]_2O\}_2$, **3**, is shown in Fig. 1b and is disposed about a crystallographic centre of inversion. The structure is constructed about a central Sn_2O_2 core, incorporating endocyclic Sn2 atoms, to which are linked two exocyclic Sn1 atoms; the O1 atom therefore, functions as a μ_3-oxo ligand. The Sn2–O1 and Sn2–O1^{i} bond lengths within the core are 2.1401(17) and 2.0427(16) Å, respectively, and are not equivalent indicating the core has the shape of a distorted diamond; symmetry operation (i): 2-x, 2-y, 2-z. The Sn1–O1 bond length of 2.0171(16) is shorter than the Sn2–O1, O1^{i} bond lengths. A further link between the exo- and endo-cyclic tin atoms is provided by a bidentate bridging carboxylate ligand with Sn1–O4 = 2.2843(18) Å and O5–Sn2^{i} = 2.2251(19) Å bond lengths indicating a close to symmetric bridge; this is verified by the experimental equivalence of the C12–O4 and C12–O5 bond lengths of 2 × 1.256(3) Å. The remaining carboxylate ligand coordinates the exocyclic Sn1 atom in the monodentate mode with the Sn1–O2 bond length being 2.1697(16) Å. Consistent with this is the Sn1···O3 separation of 2.987(3) Å and the disparity in the C1–O2 and C1–O3 bond lengths of 1.308(3) and 1.220(3) Å, respectively. The five-coordinate geometry about the Sn1 atom is based on a C_2O_3 donor set. The value of τ [61] is 0.55 indicating a significant distortion from the ideal trigonal-bipyramidal geometry, presumably owing to the close approach of the O3 atom. More striking is the coordination geometry about the Sn2 atom, ostensibly also based on a C_2O_3 donor set. However, the close approach of the O2 atom, derived from the monodentate

carboxylate ligand, at 2.7461(18) Å, clearly distorts the geometry. This is especially manifested in the wide C25–Sn2–C26 angle of 149.58(13)° which is approximately 17° wider than the C23–Sn1–C24 angle of 132.39(14)° and nearly 30° wider than the ideal angle of 120° for a trigonal-bipyramidal geometry. As a consequence, based on a C_2O_3 donor set, the value of $\tau = 0.24$ [61], indicating a considerable distortion towards a square-pyramidal geometry with the O1 atom in the apical position.

The molecular structure of hexa-nuclear $[BzSn(O)(L^1)]_6$, **4**, is shown in Fig. 1c; the molecule is disposed about an inversion centre. This "drum" molecule features two stacked six-membered Sn_3O_3 rings rotated approximately 60° relative to each other and connected by a sequence of alternating Sn–O and O–Sn bonds; the structure, therefore, features μ_3-oxo groups as for **3**. The Sn–O(oxo) bond lengths lie in the experimentally equivalent range of 2.083(2) Å, for Sn1–O2, to 2.098(3) Å, for Sn2–O1. Within the $\{Sn_3O_3\}_2$ drum, diagonally opposite tin atoms are bridged by carboxylate ligands. The carboxylate ligands are symmetrically bridging and seen in the close equivalence in the pairs of Sn–O bond lengths and associated C–O bond length collated in the caption to Fig. 1. The final position in each of the hexa-coordinate geometries is occupied by the methylene-carbon atoms derived from the tin-bound benzyl substituents. The methylene-carbon atoms are *trans* to an oxo-oxygen atom as are each of the carboxylate-oxygen atoms. Each of the resultant CO_5 coordination geometries is based on an octahedron.

The molecular structure of $Me_3Sn(L^2)OH_2$, **5**, shown in Fig. 2a. The five-coordinate geometry about the tin atom is defined by the O1 atom derived from a monodentate carboxylate ligand, the O3 atom of the water molecule and three tin-bound methyl substituents. Evidence that the carboxylate ligand is coordinating in a monodentate mode is readily seen in the disparity of the Sn–O1 and Sn–O2 separations of 2.183(2) and 3.058(3) Å, respectively, and in the difference in associated C1–O1 and C1–O2 bonds, i.e. 1.288(4) and

1.235(5) Å, respectively. The Sn–O3(water) bond length of 2.447(4) Å is intermediate between these extremes. The value of τ [61] computes to 0.83, indicating a close to *trans*-C_3O_2 trigonal-bipyramidal geometry. The minimal distortion of the *trans* O1–Sn–O3 angle, i.e. 176.12(11)°, from the ideal angle vindicates the negligible influence of the proximate O2 atom.

A one-dimensional coordination polymer is found in the structure of $[Ph_3Sn(L^2)]_n$, **6**. The asymmetric unit of **6** is represented in Fig. 2b. The carboxylate ligand is bidentate, bridging in an asymmetric mode with the Sn–O1 bond length of 2.190(2) Å being shorter than the Sn–$O2^i$ bond of 2.322(2) Å; symmetry operation (i): x, ½-y, -½+z. The closeness of the Sn–O bonds is reflected in the similarity of the C1–O1 and C1–O2 bonds of 1.274(3) and 1.251(4) Å, respectively. The *trans*-C_3O_2 coordination geometry is based on a trigonal-bipyramidal geometry with a value of τ = 0.75 [61]. The result of the bridging mode of coordination is a supramolecular coordination polymer, shown in Fig. 2c. The coordination polymer is propagated by glide-symmetry along the *c*-axis and has a zig-zag topology.

The molecular structure of $Bu_2Sn(L^2)_2$, **7**, is shown in Fig. 2d. The molecule is disposed about a two-fold axis of symmetry with the tin atom lying on the axis, relating the carboxylate ligands and n-butyl groups about the axis. The tin atom is coordinated by an asymmetrically chelating carboxylate ligand with the Sn–O1 bond length of 2.102(2) Å being shorter than Sn–O2 of 2.535(3) Å; the difference in Sn–O bond lengths is reflected in the associated C1–O1 and C1–O2 bonds of 1.306(4) and 1.221(4) Å which differ by more than 0.08 Å. The best description of the coordination geometry is one based on a skew-trapezoidal bipyramid, with the n-butyl groups orientated to lie over the weaker Sn–O2 bonds; the C13–Sn–$C13^i$ bond angle is 132.4(2)° for symmetry operation (i): 1-x, y, 1½-z. Reflecting the trapezoidal nature of the O_4 plane, the O1– Sn–O1 angle of 84.30(14)°, i.e. subtended by the short Sn–O1 bonds, is significantly narrower than the O2–Sn–O2 angle of 164.71(13)°.

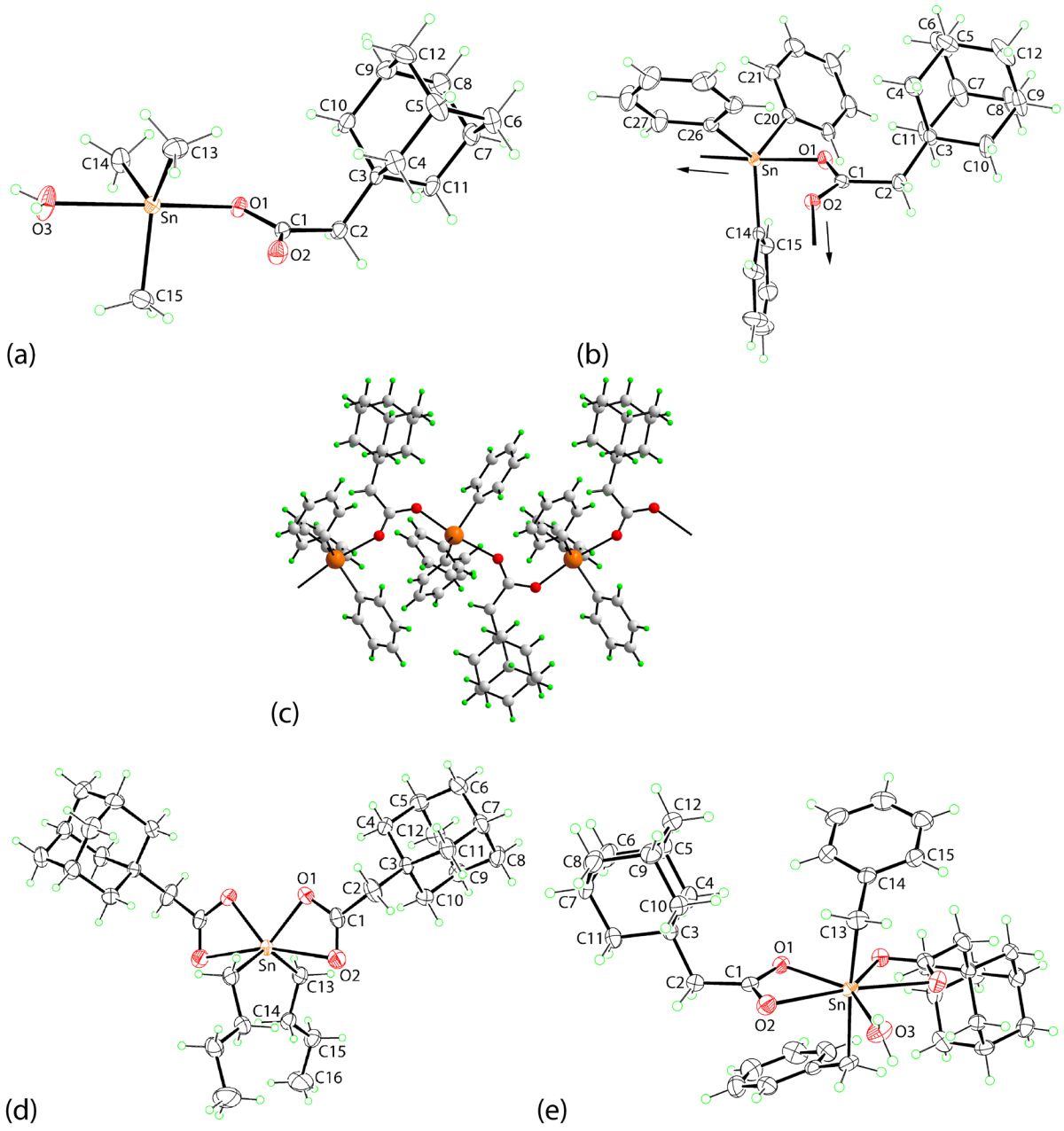

Fig. 2. The molecular structures of (a) $Me_3Sn(L^2)OH_2$ (**5**; 25% probability level), (b) $[Ph_3Sn(L^2)]_n$ (**6**; 25% probability level; the arrows indicate the links to generate the supramolecular, one-dimensional coordination polymer shown in (c)), (d) $Bu_2Sn(L^2)_2$ **7** (25% probability level) and (e) $Bz_2Sn(L^2)_2OH_2$ (**8**; 35% probability level), showing the atom labelling schemes and anisotropic displacement parameters. The unlabelled atoms are related by the symmetry operations 1-x, y, 1½-z (**7**) and 1½-x, ½-y, z (**8**).

As for **7**, the molecular structure of $Bz_2Sn(L^2)_2OH_2$, **8**, Fig. 2e, is also disposed about a two-fold axis of symmetry upon which lies the Sn and water-O3 atoms. An asymmetric mode of coordination is also noted for the independent carboxylate ligand with the Sn–O1 bond length of 2.2255(18) Å being shorter than the Sn–O2 bond of 2.387(2) Å. This disparity is significantly less than in **7** and is reflected in the near equivalence of the C1–O1 and C1–O2 bond lengths of 1.281(3) and 1.254(3) Å, respectively. The Sn-O3 bond length is 2.429(3), i.e. longer than the other Sn–O bond lengths in the molecule. The five oxygen atoms define a pentagonal plane with the methylene-carbon atoms occupying positions above and below the plane, C13–Sn–$C13^i$ is 166.60(14)°, so the coordination geometry is best described as being *trans*-C_2O_5 pentagonal-bipyramidal; symmetry operation (i): 1½-x, ½-y, z.

There are four basic structural motifs for molecules conforming to the general formula $R_3Sn(O_2CR')$ [62]. With relatively few examples of oligomeric $\{R_3Sn(O_2CR')\}_4$, exemplified by $\{(nBu)_3Sn[O_2C(2,6\text{-}C_6H_3F_2]\}_4$ [63], and $\{R_3Sn(O_2CR')\}_6$, exemplified by $\{Ph_2(Et)Sn(O_2CMe)\}_6$ [64], the predominate motifs are monomeric, as in **2**, and polymeric, as in **6**. Assuming significant bonding interactions for the second Sn–O connection in **2** (see above), the coordination geometries could be considered *cis*-C_3O_2 and *trans*-C_3O_2, respectively, for the monomeric and polymeric forms. The adoption of one form over the other can often be ascribed to steric effects in that bulky tin-bound substituents and/or carboxylate groups can mediate the formation of the Sn···O secondary bonding interaction [65,66]. The steric control over Sn···O secondary bonding interactions between tin and oxygen atoms in organotin carboxylates is well documented [67,68]. The difference between **2** and **6** in the present study is a methylene substituent in the carboxylate ligand, which is sufficient to relieve steric strain in **6**, allowing for the adoption of the observed coordination polymer. The structure of **3** conforms to the predominate structural motif for molecules of the general formula $\{[R_2Sn(O_2CR')]_2O\}_2$ [62], a commonly observed oxidation product in

organotin carboxylates, with variations to this motif found in the number of bridging carboxylate ligands [69]. Similarly, **4** conforms to the standard structural motif for molecules of the general formula $[RSn(O_2CR')O]_6$ [62]. The only literature precedent for a tin compound containing carboxylate ligands included in this study is found in the related drum structure $[nBuSn(O)(L^1)]_6$ [70]. A search of the Cambridge Structural Database [71] reveals over 80 structures related to **5**, with the first of these, i.e. $Me_3Sn(O_2CC_5H_4N\text{-}2)$, reported in 1979 [72]. There are also many literature precedents for skew-trapezoidal bipyramidal **7**, with variations relating to the asymmetry in the mode of coordination of the carboxylate ligands [73]. By contrast, there are less than 10 examples of structures conforming to pentagonal-bipyramidal **8**, with the prototype structure found in $Cy_2Sn(O_2CMe)_2(OH_2)$ [74].

3.3. Molecular packing

Based on the distance criteria assumed in PLATON [49], there are no directional interactions operating in the crystal of **2**; a view of the unit cell contents is shown in ESI Fig. S29. As for **2**, no structure-directing interactions are apparent in the crystal of **3**; a view of the unit cell contents is shown in ESI Fig. S30. The presence of the bulky adamantyl groups in **4** again precludes the formation of directional interactions in the molecular packing of **4**; a view of the unit cell contents is shown in ESI Fig. S31. The possibility of hydrogen bonding occurs in the crystal of **5** and indeed, each of the water-bound hydrogen atoms forms a hydrogen bond with symmetry-related atoms of each carboxylate-O atom; geometric parameters characterising these are given in the caption to Fig. 3. As shown in Fig. 3a, the hydrogen bonds extend laterally to form a supramolecular layer with a zig-zag topology in the *ab*-plane featuring 16-membered $\{\cdots H\cdots OCO\cdots HOSnO\}_2$ synthons. The layers stack along the *c*-axis without directional interactions between them, ESI Fig. S32.

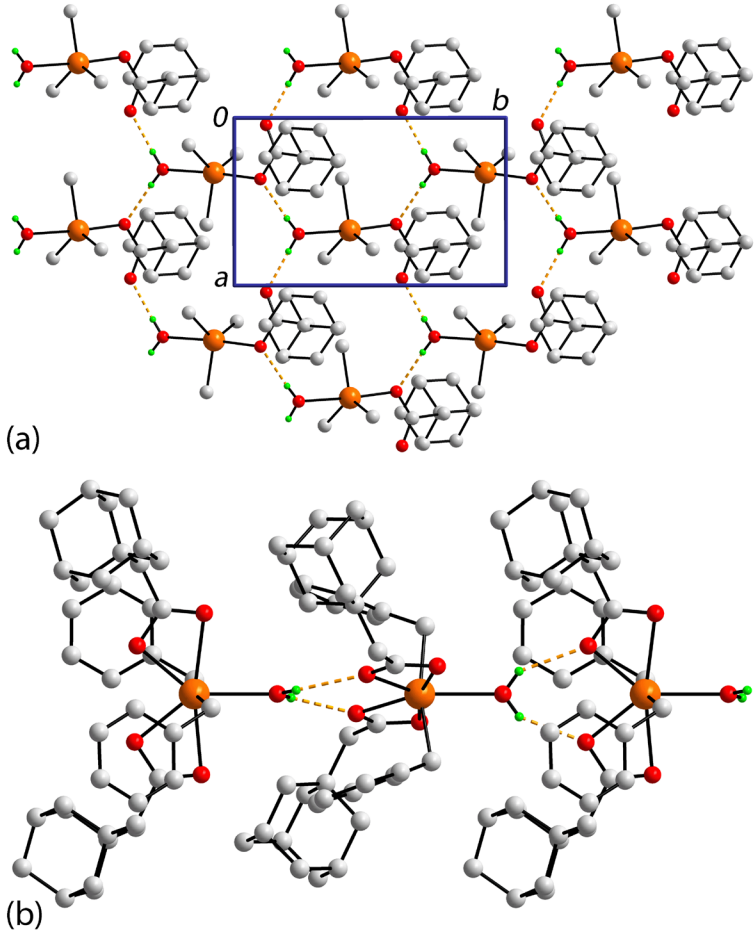

Fig. 3. Molecular packing sustained by hydrogen bonding in the crystals of **5** and **8**: (a) **5**, a view of the supramolecular layer in the *ab*-plane sustained by water-O–H···O(carboxylate) hydrogen bonding and (b) a view of the zig-zag supramolecular chain along the *c*-axis sustained water-O–H···O(carboxylate) hydrogen bonding. Non-participating hydrogen atoms have been omitted for reasons of clarity.

Geometric (Å, °) details of the intermolecular interactions:

5

A	H	B	A–H	H···B	A···B	A–H···B	Symmetry operation
O3	H1o	O2	0.82(3)	1.88(3)	2.699(4)	175(8)	-x, ½+y, ½-z
O3	H2o	O1	0.82(4)	1.99(4)	2.807(4)	176(3)	1-x, ½+y, ½-z

8

O3	H1o	O1	0.82(3)	2.14(3)	2.858(3)	147(3)	x, ½-y, -½+z

The one-dimensional coordination polymer formed in crystals of **6** packs with no specific atom-to-atom contacts between them; a view of unit cell contents is shown in ESI Fig. S33. From the image in ESI Fig. S34, it clearly apparent that there are no directional interactions stabilising the molecular packing in the crystal of **7**. Hydrogen bonding comes to the fore again in the crystal of **8**; geometric parameters characterizing these are given in the caption to Figure 3. The tin-bound water molecule functions as the donor to the more tightly bound O1 atoms to form a supramolecular chain along the *c*-axis with a zig-zag topology, being propagated by glide-symmetry, see Figure 3b; as shown in ESI Fig. S35, supramolecular chains assemble with no directional interactions between them.

From the foregoing, it is apparent the large adamantyl groups exert a great influence upon the molecular packing, primarily keeping the constituent species apart. To analyse the influence of the adamantyl groups further, an analysis of the molecular packing was conducted employing CrystalExplorer 17.0[75] and following established protocols.[76] Specifically, the Hirshfeld surfaces and two-dimensional fingerprint plots were calculated for **2**-**8** in order to determine the nature of the specific atom-to-atom contacts between molecules in their respective crystals, even though the separations are usually greater than the respective sums of the van der Waals radii, as indicated above with the notable exception of the structures of **5** and **8** where hydrogen-bonding apparent.

The first structures to be highlighted are the triphenyltin species **2** and **6**. In mononuclear **2**, H···H contacts contribute 70.1% to the overall calculated Hirshfeld surface with the next most prominent contacts being C···H/H···C at 24.8%; next are O···H/H···O at 4.5%. These values are comparable to those calculated for the repeat unit in polymeric **6**, i.e. 71.6, 23.7 and 2.6% for H···H, C···H/H···C and O···H/H···O surface contacts, respectively. The only other contact of note is due to the secondary Sn···O bonding interaction, i.e. 1.5%. The calculations were then repeated for a six repeat-unit fragment of the polymer. In consideration of packing of the one-

dimensional chains, the H···H surface contacts increased to 79.6%, largely at the expense of C···H/H···C (17.3%), O···H/H···O (1.2%) and Sn···O/O···Sn (0.0%) contacts. The only other structure without hydrogen-bonding potential but, with phenyl rings, giving rise to the possibility of C···H contacts, is hexa-nuclear **4** where H···H (86.6%), C···H/H···C (10.3%) and O···H/H···O (2.6%) surface contacts dominate. In tetra-nuclear **3**, H···H contacts overwhelming dominate the calculated Hirshfeld surface, contributing 93.2%; O···H/H···O and C···H/H···C contacts are next at 6.1 and 0.6%, respectively. A similar situation pertains in **7**, with H···H (88.8%) and O···H/H···O (10.8%), being the only surface contacts contributing more than 1%. The two remaining structures feature conventional water-O–H···O(carboxylate) hydrogen-bonding interactions. Similar trends observed above are evident. Thus, in **5**, without phenyl rings, the dominance of H···H (90.1%) is clear, with O···H/H···O contacts (9.1%) being the only other significant contributor to the Hirshfeld surface. In **8**, with tin-bound benzyl substituents, H···H contacts fall off to 79.6% with C···H/H···C (10.4%) and O···H/H···O (10.0%) being approximately equal and making up the balance of surface contacts.

3.4 Anti-bacterial activity results and preliminary assessment of cytotoxicity

In order to ascertain the potential of the new organotin compounds as anti-bacterial agents, a variety of trials were conducted on organotin derivative **1**, **2** and **5**-**7**, pro-ligands HL^1 and HL^2 as well as the organotin precursors, i.e. Me_3SnCl (**S1**), Ph_3SnOH (**S2**) and Bu_2SnCl_2 (**S3**), and standard anti-biotics Tetracycline and Chloramphenicol. The screening protocols employed in the present study followed a literature precedent [77].

3.4.1. Disc diffusion screening

The trial compounds were first screened using the Kirby-Bauer disc diffusion method with the results summarised in Table 2. All compounds were evaluated as freshly prepared

DMSO solutions; DMSO was included in all assays as the solvent control and exhibited no anti-bacterial activity on any of the bacterial species. The pro-ligands, HL^1 and HL^2, exhibited no effect against any of the panel of bacteria. In the same way, the trimethyltin chloride (**S1**) precursor had no effect on the bacteria. However, the precursors triphenyltin hydroxide (**S2**) and dibutyltin dichloride (**S3**) exhibited anti-bacterial activities on most species, especially on Gram-positive species having inhibition zones in the ranges 14-20 and 11-18 mm, respectively. Against Gram-negative bacteria, **S3** was effective against all species, except *P. aeruginosa*, whereas **S2** was moderately effective against a limited number of the species, being most potent against *V. parahaemolyticus* (14 mm).

Insert Table 2

As observed for their precursor, **S1**, trimethyltin derivatives, **1** and **5**, demonstrated no anti-bacterial activity against all tested species with the exception of **5** against *S. aureus* (MRSA) (7 mm). This observation suggests that there is no contribution to the bioactivity by the incorporation of the ligands L^1 and L^2. By contrast and similar to their precursor **S2**, triphenyltin derivatives **2** and **6** demonstrated anti-bacterial effects against both Gram-positive and Gram-negative bacteria. However, as for the trimethyltin derivatives, the formation of triphenyltin derivatives **2** and **6** did not show improvement in their bacterial inhibition activity. Compound **2** was equally effective against all tested Gram-positive species with inhibition zones ranging from 12-18 mm in diameter. Notably, **2** was only effective against two Gram-negative bacterial species, *V. parahaemolyticus* (12 mm) and *S. flexneri* (7mm). Compared to **2**, **6** exerted reduced anti-bacterial activities against all Gram-positive and was inactive against *E. faecium*. Limited activity was observed against two Gram-negative bacterial species, i.e. *P. vulgaris* (10 mm) and *V. parahaemolyticus* (10 mm). Finally, **7** demonstrated similar anti-bacterial effects as for **6** but, was equal to or less potent than precursor **S3**. Compound **7** exerted mild anti-bacterial activities against all Gram-

positive species except *E. faecium* and was only effective against two Gram-negative bacteria, *S. flexneri* and *V. parahaemolyticus*, each with a 10 mm inhibition zone.

The standard anti-biotics, Tetracycline and Chloramphenicol were employed (each with 30 μg per disc) in the experiment as positive controls. Each anti-biotic produced inhibition zones ranging from 26-33 and 24-30 mm, respectively, against Gram-positive bacteria, and 9-25 and 11-29 mm, respectively, against Gram-negative species.

In summary, the results from the disc diffusion anti-bacterial activity screening suggested that trimethyltin derivatives **1** and **5** were inactive, while **2**, **6** and **7** exhibit broad spectrum anti-bacterial activities against both Gram-positive and Gram-negative bacteria, similar but, less potent that their respective precursors **S2** and **S3**. In comparing the potency of the organotin compounds with the standard anti-biotics, the former compounds are not as effective as the anti-biotics when same concentrations were employed in the assay.

3.4.2. Determination of Minimum Inhibitory Concentration (MIC) and Minimum Bactericidal Concentration (MBC)

As demonstrated in the disc diffusion assay, three of the organotin derivatives, **2**, **6** and **7**, and their respective precursors (**S2** and **S3**), showed potential in inhibiting bacterial growth (Table 2). The anti-bacterial activity of these compounds was quantitatively evaluated using the broth-dilution method. The MIC and MBC values of these compounds against eight species, including six Gram-positive (*E. faecalis*, *S. pyogenes*, *S. epidermidis, S. aureus* (MRSA), *E. faecium* and *S. pneumoniae*) and two Gram-negative (*S. flexneri* and *V. parahaemolyticus*) species, was tested. Tetracycline and Chloramphenicol were included as positive controls.

In the MIC assay, striking differences are noted in the anti-bacterial potency exhibited by the triphenyltin species (**2**, **6** and **S2**) compared with the di-n-butyl species (**7** and **S3**),

Table 3. While the trend seen in the disc diffusion results is retained whereby the precursor (**S3**) is more potent than the dibutyltin derivative **7**, neither are as potent as any of the triphenyltin compounds. The precursor **S2** exhibited maximum and equivalent anti-bacterial activity, i.e. 0.78 µg/mL, against four Gram-positive bacteria (*E. faecalis*, *S. aureus* (MRSA), *S. epidermidis* and *S. pyogenes*) and one Gram-negative bacterium (*V. parahaemolyticus*). Comparable activity was evident for **2** and **6** in most of Gram-negative bacteria but, not against the Gram-negative bacteria. Thus, **2** and **6** each exhibited the same level of activity as **S2**, i.e. 0.78 µg/mL, against *S. epidermidis* and *S. pyogenes*; **2** was also potent against *S. aureus* (MRSA), again with a MIC value of 0.78 µg/mL. Notably, **2** remained as the most effective compound among the tested organotin compound. In summary, the MIC data confirmed the potent anti-bacterial activity of the triphenyltin derivatives as observed in disc diffusion assay.

Insert Table 3

After determining the anti-bacterial activities of the organotin derivatives, the compounds were further studied to identify their abilities either to kill (bactericidal) a bacterium or to inhibit the growth (bacteriostatic) of a bacterium as revealed from the obtained MBC/MBC ratios. An anti-bacterial agent is considered bactericidal if the value of MBC is not four-fold greater than the MIC value, i.e. MBC/MIC ≤4 [78]. In the present study, Tetracycline demonstrated bactericidal activities against *S. epidermidis* and *S. pyogenes* but, was bacteriostatic towards the remaining bacteria, Table 3; Chloramphenicol was bactericidal towards only *S. pyogenes* only. For **S2**, with the exception against *S. pneumoniae*, the MBC values observed in all tested species were more than 4-fold greater than their respective MIC values, indicating **S2** to be generally bacteriostatic. By contrast, the anti-bacterial activities of organotin derivatives, **2** and **6** were proven to be bactericidal against *E. faecalis* and Gram-negative *V. parahaemolyticus*. The dibutyltin compound, **7**,

while not especially potent, was able to kill both *S. pneumoniae* and *V. parahaemolyticus* while its precursor, **S3**, was only able to kill *V. parahaemolyticus*.

3.4.3. Time-kill assay

Following MIC and MBC determinations, time-kill assays were conducted to reveal the potential pharmacodynamics of the triphenyltin derivatives **2** and **6** as they were shown to be the most potent agents against *S. pyogenes*, *S. epidermidis* and *S. aureus* (MRSA), with MIC values of 0.78 μg/ml (Table 3). The anti-bacterial effects of **2** and **6** were studied at various incubation time-points, specifically 0, 1, 2, 4, 8 and 24 h. At all three tested concentrations (½ × MIC, 1 × MIC and 2 × MIC), **2** was able to suppress the growth of *S. pyogenes* for 8 h, followed by a spike in growth with the exception of bacteria treated with 2 × MIC, Fig. 4a. A similar response was noted against *S. epidermidis* except growth of the 2 × MIC-treated bacterium after 8 h, Fig. 4b. For *S. aureus* (MRSA), the growth was inhibited for 8 h at MIC and 2 × MIC, but for only 2 h at ½ × MIC, Fig. 4c.

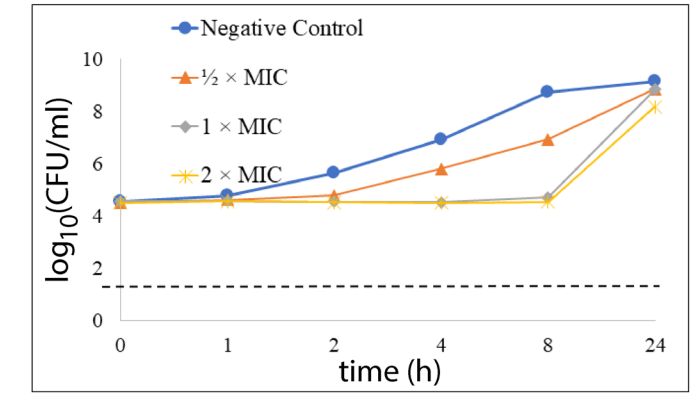

(c)

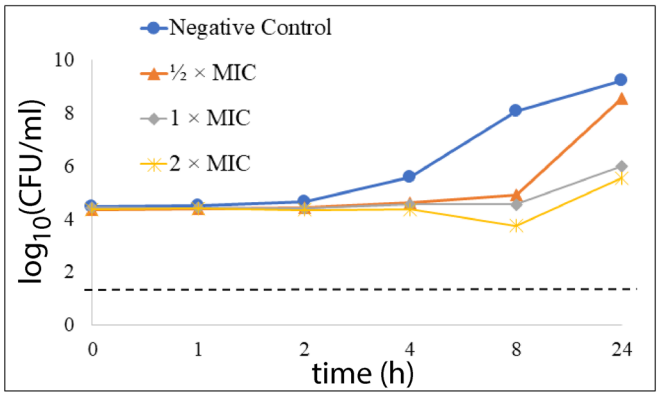

(b)

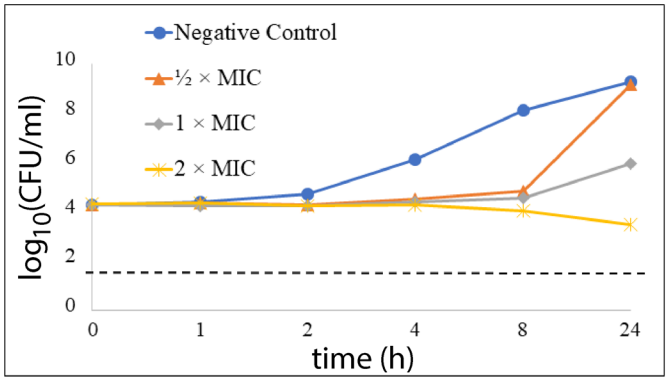

(a)

Fig. 4. Time-kill curves for **2** against (a) *S. pyogenes*, (b) *S. epidermidis* and (c) *S. aureus* (MRSA). The bactericidal level is indicated by the dashed line - - -, negative control ●, ½ × MIC ▲, 1 × MIC ♦ and 2 × MIC ×.

To a first approximation, **6** gave similar time-kill responses as for **2** against both *S. pyogenes* and *S. epidermidis*. Against, *S. pyogenes*, Figure 5a, and *S. epidermidis*, Fig. 5b, growth was maintained for 4 h at ½ × MIC and two additional hours at both MIC and 2 ×

MIC. A summary of the bacterial count numbers at different concentrations and time-points is presented in Table 4.

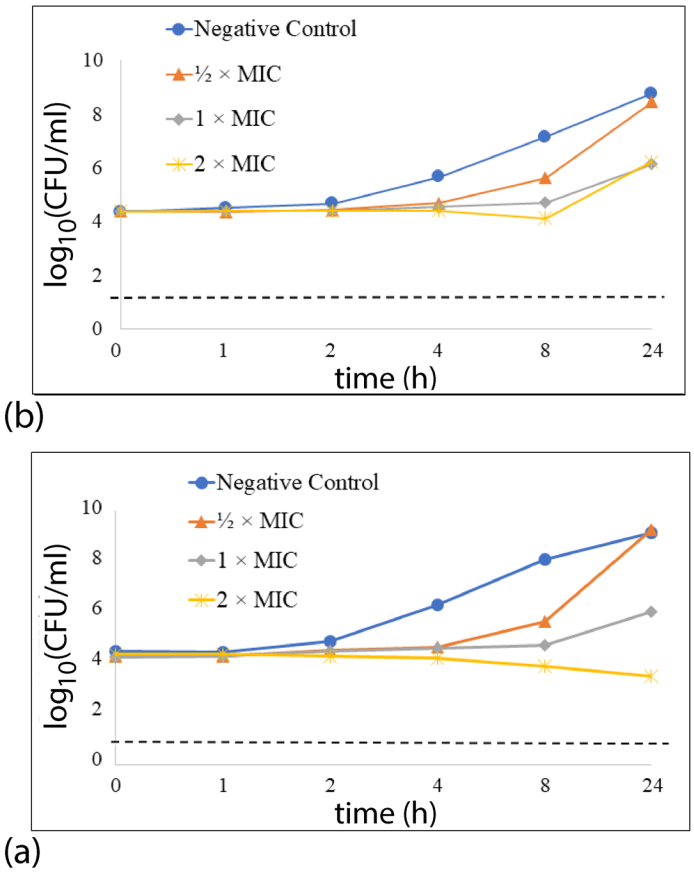

Fig. 5. Time-kill curves for **6** against (a) *S. pyogenes* and (b) *S. epidermidis*. The bactericidal level is indicated by the dashed line - - -, negative control ●, ½ × MIC ▲, 1 × MIC ♦ and 2 × MIC ×.

Typically, anti-biotics are classified into two classes, those that are bactericidal, i.e. able to kill bacteria, and those that are bacteriostatic, i.e. able to inhibit bacterial growth. Conventionally, bactericidal anti-biotics are preferred for patients who are severely ill or immunosuppressed, as reflected in the guidelines for anti-biotic use [79]. The present results showed that the anti-bacterial activity of **2** and **6** was bacteriostatic towards the bacterial species tested. Although having bactericidal activity might be thought desirable, a systematic

review and meta-analysis conducted in 2014 suggested that the categorisation of bacteriostatic and bactericidal anti-biotics is most likely irrelevant in clinical practice as there was no correlation between the use of bactericidal agents and clinical cure rates and mortality rates [80]. In summary, the anti-bacterial effects of **2**, **6**, **7**, **S2** and **S3** were broad spectrum, targeting both Gram-positive and Gram-negative bacteria. Based on time-kill studies, **2** and **6** exhibited bacteriostatic effects on selected bacteria tested.

Insert Table 4

3.4.4. Cytotoxicity assay

As a preliminary evaluation of the toxicity of the compounds towards mammalian cells, cytotoxicity screening was conducted on a representative cell line, HEK293T, i.e. a human embryonic kidney cell line, using the MTT proliferation assay. All test compounds exhibited dose-dependent cytotoxic effects with the results summarised in Table 5; graphs are presented in ESI Fig. S36. The pro-ligands HL^1 and HL^2 were non-cytotoxic, maintaining >80% cell viability at 100 µg/mL. However, the organotin derivatives and precursors exhibited cytotoxic effects, with $\log_{10}(CC_{50})$ values ranging from 0.079 to 1.579 µg/mL. The trimethyltin derivatives, **1** and **5**, were least toxic to normal cells. By contrast, the potent anti-bacterial agents **2** and **6** were cytotoxic towards HEK293T, demonstrating low $\log_{10}(CC_{50})$ values of 0.079 ± 0.035 and 0.084 ± 0.046 µg/mL, respectively. The dibutyltin dichloride precursor, **S3**, was the most cytotoxic to HEK293T among the tested compounds but, **7** was less so, i.e. $\log_{10}(CC_{50}) = 0.421 \pm 0.045$ µg/mL.

Insert Table 5

3.4.5. Overview of anti-bacterial assays

Described as a "lipophilic bullet" in their seminal review of the pharmacological potential of adamantane derivatives, being second only to methyl in its impact, Wanka and Schreiner highlighted the potential of appending adamantane-containing molecules to already active pharmaceutical ingredients (API's) to enhance their therapeutic value [5]. The anti-bacterial activity of organotin derivatives, including organotin carboxylates, is already well-documented [33] so it seemed a natural step forward to evaluate the anti-bacterial potential of a variety of organotin species coupled with adamantane carboxylates. Further, broad-spectrum anti-bacterial behaviour exhibited by adamantane-1-carbohydrazides in contrast to limited anti-fungal activity was ascribed to the lipophilic attributes of the molecules [81]. Previous mechanistic studies highlighted the important role of lipophilic agents to interact and penetrate into the phospholipid membrane of bacteria hence, disrupting the membrane structure and crucial biological functions essential for cell survival [82].

Based on the new results, triphenyltin compounds such as **2** and **6** are better anti-bacterial agents compared to trimethyltin compounds (**1** and **5**), regardless of the specific ligand employed. Dibutyltin derivative, **7**, demonstrated moderate anti-bacterial activity. It has been reported that the organotin derivatives containing phenyl substituents generally exert better anti-bacterial activity compared to compounds with methyl and butyl substituents [83]. The enhanced anti-bacterial activity for the triphenyltin derivatives may be attributed to an increase in the lipophilicity of these compounds which may facilitate their entry into the lipid bilayer of bacterial cell membrane before exerting the observed anti-bacterial effects.

The results showed that some of the organotin compounds were as effective as commercially available anti-biotics. When the anti-bacterial activity of the new organotin compounds was screened using disc diffusion assays, they appeared to be less effective in terms of their anti-microbial activity compared with both tetracycline and chloramphenicol.

However, when tested using the broth dilution method, the gold standard method for anti-microbial screening assay, the MIC results showed that although the potent anti-bacterial agent tetracycline consistently out-performed each of **2**, **6** and **7**, triphenyltin compounds **2** and **6** had lower MIC values on Gram-positive bacteria including *E. faecium*, *MRSA*, *S. epidermidis*, *S. pyogenes* and *S. pneumoniae* compared to chloramphenicol, indicating that **2** and **6** are potentially novel anti-bacterial agents for these pathogens. Existing anti-biotics such as chloramphenicol are losing their effectiveness in certain bacteria, for instance, *MRSA*. The development of organotin compounds, such as **2** and **6**, presents new alternatives to infectious diseases caused by multi-drug resistant bacteria.

4. Conclusion

A series of nine diamondoid-decorated organotin(IV) derivatives were prepared by reacting two adamantyl carboxylic acids, or their sodium salts, with tin precursors containing various organic groups. FT-IR and ^{1}H NMR confirmed Sn–O bond formation between the carboxylate group of the ligand and the organotin moiety. X-ray crystallography and ^{119}Sn NMR indicated the hexa-coordinate drum structure of the monoorganostannoxanes $[BzSn(O)(L^{1})]_6$ (**4**) and the structure $[BzSn(O)(L^{2})]_6$ (**9**) are retained in solution, whereas the solid-state five-coordinate monomer or polymeric structures of triganostannoxanes $Me_3Sn(L^{1})$ (**1**), $Ph_3Sn(L^{1})$ (**2**), $Me_3Sn(L^{2})OH_2$ (**5**) and $[Ph_3Sn(L^{2})]_n$ (**6**) are four-coordinate in solution. The diorganostannoxes $\{[Me_2Sn(L^{1})]_2O\}_2$ (**3**) and $Bu_2Sn(L^{2})_2$ (**7**) form ladder and trapezoidal bipyramid structure, respectively, that are retained in solution, while $Bz_2Sn(L^{2})_2OH_2$ (**8**) probably dissociates water in solution to give a hexa-coordinate species. The presence of water in compounds **5** and **8** results in hydrogen bonding, giving rise to supramolecular layer with a zig-zag topology (**5**) and a zig-zag chain (**8**). The anti-bacterial effects of selected organotin compounds showed that the triphenyltin derivatives **2** and **6** exhibited promising broad-spectrum, anti-bacterial effects with maximum

potency towards *S. pyogenes*, *S. epidermidis* (**2** and **6**) and *S. aureus* (MRSA) (**2**). Time-kill assays proved **2** and **6** to be bacteriostatic against these bacteria. Despite being cytotoxic towards normal cells, the new results suggest further studies in this area are warranted.

Conflict of interest

The authors declare that they have no conflicts of interest with the contents of this article.

Acknowledgements

This research received financial support from the Department of Biotechnology, India (Grant No. BT/PR 25263/NER/95/1104/2017, TSBB) and Sunway University Sdn Bhd (Grant no. GRTIN-IRG-01-2021). TSBB and RM acknowledge access to DST-PURSE for the diffractometer facility.

Appendix A. Supplementary data

CCDC-1921532-1921538 contains the supplementary crystallographic data for compounds **2-8** reported in this paper. These data can be obtained free of charge via http://www.ccdc.cam.ac.uk/conts/retrieving.html, or from the Cambridge Crystallographic Data Centre, 12 Union Road, Cambridge CB2 1EZ, UK; fax: (+44) 1223-336-033; or e-mail: deposit@ccdc.cam.ac.uk.

Supplementary data associated with this article can be found, in the online version, at http:// XXXX. IR, ^{1}H, ^{13}C and ^{119}Sn NMR spectra (Figs. S1-S28). X-ray: Unit cell contents (Figs. S29-S35) and graphs of MTT assay (Fig. S36).

References

[1] R. C. Fort, Adamantane: The Chemistry of Diamond Molecules, Marcel Dekker, New York, USA, 1976.

[2] H. Schwertfeger, A. A. Fokin, P. R. Schreiner, Angew. Chem. Int. Ed. 47 (2008) 1022-1036.

[3] M. A. Gunawan, J.-C. Hierso, D. Poinsot, A. A. Fokin, N. A. Fokina, B. A. Tkachenko, P. R. Schreiner, New J. Chem. 38 (2014) 28-41.

[4] J. Liu, D. Obando, V. Liao, T. Lifa, R. Codd, Eur. J. Med. Chem. 46 (2011) 1949-1963.

[5] L. Wanka, K. Iqbal, P.R. Schreiner, Chem. Rev. 113 (2013) 3516-3604.

[6] Š. Horvat, K. Mlinarić-Majerski, L. Glavaš-Obrovac, A. Jakas, J. Veljković, S. Marczi, G. Kragol, M. Roščić, M. Matković, A. Milostić-Srb, J. Med. Chem. 49 (2006) 3136-3142.

[7] M. Roščić, V. Sabljić, K. Mlinarić-Majerski, Š. Horvat, Croat. Chem. Acta 81 (2008) 637-640.

[8] A. Perl, A. Gomez-Casado, D. Thompson, H.H. Dam, P. Jonkheijm, D.N. Reinhoudt, J. Huskens, Nat. Chem. 3 (2011) 317-322.

[9] B.-W. Liu, H. Zhou, S.-T. Zhou, J.-Y Yuan, Eur. Polym. J. 65 (2015) 63-81.

[10] A. Štimac, M. Šekutor, K. Mlinarić-Majerski, L. Frkanec, R. Frkanec, Molecules 22 (2017) art. no. 297; doi:10.3390/molecules22020297

[11] J. R. Schnell, J. J. Chou, Nature 451 (2008) 591-595.

[12] S. D. Cady, W. Luo, F. Hu, M. Hong, Biochemistry 48 (2009) 7356-7364.

[13] C. F. Chew, A. Guy, P. C. Biggin, Biophys. J. 95 (2008) 5627-5636.

[14] G. Lamoureux, G. Artavia, Curr. Med. Chem. 17 (2010) 2967-2978.

[15] (a) M. Grillaud, A. Bianco, J. Pept. Sci. 21 (2015) 330-345; (b) G. Lamanna, M. Grillaud, C. Macri, O. Chaloin, S. Muller, A. Bianco, Biomaterials 35 (2014) 7553-7561.

[16] (a) G. Lamanna, C. R. Smulski, N. Chekkat, K. Estieu-Gionnet, G. Guichard, S. Fournel,

A. Bianco, Chem.-Eur. J. 19 (2013) 17621768; (b) G. Lamanna, J. Russier, H. Dumortier, A. Bianco, Biomaterials 33 (2012) 5610-5617.

[17] M. Grillaud, J. Russier, A. Bianco, J. Am. Chem. Soc. 136 (2014) 810-819.

[18] M. Grillaud, A. P. Ruiz de Garibay, A. Bianco, RSC Adv. 6 (2016) 42933-42942.

[19] H. Hu, C. Lin, M. Ao, Y. Ji, B. Tang, X. Zhou, M. Fang, J. Zeng, Z. Wu, RSC Adv. 7 (2017) 51640-51651.

[20] V. Burmistrov, C. Morisseau, K. S. S. Lee, D. S. Shihadih, T. R. Harris, G. M. Butov, B. D. Hammock, Bioorg. Med. Chem. Lett. 24 (2014) 2193-2197.

[21] M. M. Đorđević, D. A. Jeremić, M. V. Rodić, V. S. Simić, I. D. Brčeski, V. M. Leovac, Polyhedron 68 (2014) 234-240.

[22] V. M. Leovac, M. V. Rodić, L. S. Jovanović, M. D. Jovanović, T. Stanojković, M. Vujčić, D. Sladić, V. Marković, L. S. Vojinović-Ješić, Eur. J. Inorg. Chem. (2015) 882-895.

[23] J. Jimenez, I. Chakraborty, M. Rojas-Andrade, P.K. Mascharak, J. Inorg. Biochem. 168 (2017) 13-17.

[24] (a) H. Schwertfeger, A. A. Fokin, P. R. Schreiner, Angew. Chem., Int. Ed. 47 (2008) 1022-1036. (b) M. A. Gunawan, J. C. Hierso, P. R. Schreiner, New J. Chem. 38 (2014) 28-41.

[25] (a) S. Fujii, U. Akiba, M. Fujihira, J. Am. Chem. Soc. 124 (2002) 13629-13635. (b) T. Kitagawa, Y. Idomoto, H. Matsubara, D. Hobara, T. Kakiuchi, T. Okazaki, K. Komatsu, J. Org. Chem. 71 (2006) 1362-1369.

[26] B. E. K. Barth, B. A. Tkachenko, J. P. Eußner, P. R. Schreiner, S. Dehnen, Organometallics 33 (2014) 1678-1688.

[27] Z. A. K. Khattak, H. A. Younus, N. Ahmad, B. Yu, H. Ullah, S. Suleman, A. H. Chughtai, B. Moosavi, C. Somboon, F. Verpoort, J. CO_2 Util. 28 (2018) 313-318.

[28] A. V. Gurbanov, M. F. C. Guedes da Silva, L. M. Kustov, F. I. Guseinov, K. T.

Mahmudov, A. J. L. Pombeiro, J. Organomet. Chem. 867 (2018) 98-101.

[29] R. Shankar, A. Dubey, A. K. Jassal, E. Jakhar, G. Kociok-Köhn, Inorg. Chem. 58 (2019) 10955-10964.

[30] T. S. Basu Baul, A. Chaurasiya, A. Duthie, P. Montes-Tolentino, H. Höpfl, Cryst. Growth. Des. 19 (2019) 6656-6671.

[31] C. N. Banti, S. K. Hadjikakou, T. Sismanoglu, N. Hadjiliadis, J. Inorg. Biochem. 194 (2019) 114-152.

[32] J. Ordóñez-Hernández, R. Arcos-Ramos, H. García-Ortega, E. Munguía-Viveros, M. Romero-Ávila, M. Flores-Alamo, I. Gracia-Mora, F. Sánchez-Bartéz, R. Santillan, N. Farfán, J. Mol. Struct. 1180 (2019) 462-471.

[33] T. S. Basu Baul, Appl. Organomet. Chem. 22 (2008) 195-204.

[34] J. O. Adeyemi, D. C. Onwudiwe, A. C. Ekennia, C. P. Anokwuru, N. Nundkumar, M. Singh, E. C. Hosten, Inorg. Chim. Acta 485 (2019) 64-72.

[35] V. K. Choudhary, A. K. Bhatt, D. Dash, N. Sharma, Appl. Organomet. Chem. 34 (2020) e5360.

[36] C. L. Xing, Y. Fang, L. Jiang, Y.-H. Zhang, M.-X. Li, J. Organomet. Chem. 911 (2020) 121153.

[37] A. S. L. Barbosa, J. D. Guedes, D. R. da Silva, S. M. P. Meneghetti, M. R. Meneghetti, A. E. da Silva, M. V. de Araujo, M. S. Alexandre-Moreira, T. M. de Aquino, J. P. de Siqueira Jr, R. S. A. de Araújo, R. M. D. da Cruz, F. J. B. Mendonça Jr, J. Inorg. Biochem. 180 (2018) 80-88.

[38] P. Debnath, A. Das, K. S. Singh, T. Yama, S. S. Singh, R. J. Butcher, L. Sieroń, W. Maniukiewicz, Inorg. Chim. Acta 498 (2019) 119172.

[39] M. P. Chrysouli, C. N. Banti, N. Kourkoumelis, E. E. Moushi, A. J.Tasiopoulos, A. Douvalis, C. Papachristodoulou, A. G. Hatzidimitriou, T. Bakase, S. K. Hadjikakou, Dalton Trans. 49 (2020) 11522.

[40] C. D. Britten, E. Garrett-Mayer, S. H. Chin, K. Shirai, B. Ogretmen, T. A. Bentz, A. Brisendine, K. Anderton, S. L. Cusack, L. W. Maines, Y. Zhuang, C. D. Smith, M. B. Thomas, Clin. Cancer Res. 23 (2017) 4642-4650.

[41] W.L.F. Armarego, C. L. L. Chai, Purification of Laboratory Chemicals, 7th ed.; Butterworth-Heinemann, Oxford, U. K., 2012.

[42] B. Kushlefsky, I. Simmons, A. Ross, Inorg. Chem. 2 (1963) 187-189.

[43] K. Sisido, T. Takeda, J. Kinigawa, J. Am. Chem. Soc. 83 (1961) 538-541.

[44] Agilent Technologies, CrysAlisPro, Santa Clara, CA, USA, 2013.

[45] G. M. Sheldrick, Acta Crystallogr. Sect. A 64 (2008) 112-122.

[46] G. M. Sheldrick, Acta Crystallogr. Sect. C 71 (2015) 3-8.

[47] L. J. Farrugia, J. Appl. Crystallogr. 45 (2012) 849-854.

[48] DIAMOND, Visual Crystal Structure Information System, Version 3.1, Crystal Impact, Postfach 1251, D-53002 Bonn, Germany, 2006.

[49] A. L. Spek, Acta Crystallogr. Sect. D 65 (2009) 148-155.

[50] T. S. Basu Baul, A. Paul, L. Pellerito, M. Scopelliti, A. Duthie, D. de Vos, R. P. Verma, U. Englert, J. Inorg. Biochem. 107 (2012) 119-128.

[51] T. S. Basu Baul, C. Masharing, S. Basu, E. Rivarola, M. Holčapek, R. Jirásko, A. Lyčka, D. De Vos, A. Linden, J. Organomet. Chem. 691 (2006) 952-965.

[52] T. S. Basu Baul, W. Rynjah, E. Rivarola, A. Lyčka, M. Holčapek, R. Jirásko, D. De Vos, R. J. Butcher, A. Linden, J. Organomet. Chem. 691 (2006) 4850-4862.

[53] P. G. Harrison, in: P. G. Harrison (Ed.), Chemistry of Tin, Chapman and Hall, New York, 1989.

[54] R. Willem, I. Verbruggen, M. Gielen, M. Biesemans, B. Mahieu, T. S. Basu Baul, E. R. T. Tiekink, Organometallics 17 (1998) 5758-5766.

[55] J. Holeček, M. Nádvorník, K. Handlíř, A. Lyčka, J. Organomet. Chem. 315 (1986) 299-308.

[56] T. S. Basu Baul, A. Paul, L. Pellerito, M. Scopelliti, P. Singh, P. Verma, A. Duthie, D. de Vos, E. R. T. Tiekink, Investg. New Drugs 29 (2011) 285-299.

[57] T. S. Basu Baul, C. Masharing, E. Rivarola, F. E. Smith, R. J. Butcher, Struct. Chem. 18 (2007) 231-235.

[58] T. S. Basu Baul, A. Mizar, X. Song, G. Eng, R. Jirásko, M. Holčapek, R. Willem, M. Biesemans, I. Verbruggen, R. Butcher, J. Organomet. Chem. 691 (2006) 2605-2613.

[59] V. Chandrasekhar, K. Gopal, S. Nagendran, A. Steiner, S. Zacchini, Cryst. Growth Des. 6 (2006) 267-273.

[60] V. Chandrasekhar, K. Gopal, P. Singh, R. S. Narayanan, A. Duthie, Organometallics 28 (2009) 4593-4601.

[61] A. W. Addison, T. N. Rao, J. Reedijk, J. van Rijn, G. C. Verschoor, J. Chem. Soc. Dalton Trans. (1984) 1349-1356.

[62] E. R. T. Tiekink, Appl. Organomet. Chem. 5 (1991) 1-23.

[63] M. Gielen, A. El Khloufi, M. Biesemans, F. Kayser, R. Willem, B. Mahieu, D. Maes, J. N. Lisgarten, L. Wyns, A. Moreira, T. K. Chattopadhay, R. A. Palmer, Organometallics 13 (1994) 2849-2854.

[64] M. M. Amini, A. Azadmeher, V. Alijani, H. R. Khavasi, T. Hajiashrafi, A. N. Kharat, Inorg. Chim. Acta 362 (2009) 355-360.

[65] N. W. Alcock, Adv. Inorg. Chem. Radiochem. 15 (1972) 1-58.

[66] E. R. T. Tiekink, Coord. Chem. Rev. 345 (2017) 209-228.

[67] R. Willem, I. Verbruggen, M. Gielen, M. Biesemans, B. Mahieu, T. S. Basu Baul, E. R. T. Tiekink, Organometallics 17 (1998) 5758-5766.

[68] D. Dakternieks, A. Duthie, D. R. Smyth, C. P. D. Stapleton, E. R. T. Tiekink, Organometallics 22 (2003) 4599-4603.

[69] J. Beckmann, D. Dakternieks, F. S. Kuan, E. R. T. Tiekink, J. Organomet. Chem. 659 (2002) 73-83.

[70] V. Chandrasekhar, V. Baskar, R. Boomishankar, K. Gopal, S. Zacchini, J. F. Bickley, A. Steiner, Organometallics 22 (2003) 3710-3716.

[71] C. R. Groom, I. J. Bruno, M. P. Lightfoot, S. C. Ward, Acta Crystallogr. B 72 (2016) 171-179.

[72] P. G. Harrison, R. C. Philips, J. Organomet. Chem. 182 (1979) 37-46.

[73] T. S. Basu Baul, A. Paul, E. R. T. Tiekink, Acta Crystallogr. Sect. E 67 (2011) m1383-m1384.

[74] D. Dakternieks, F. S. Kuan, E. R. T. Tiekink, Main Group Met. Chem. 24 (2001) 291-292.

[75] Crystal Explorer v17, M. J. Turner, J. J. Mckinnon, S. K. Wolff, D. J . Grimwood, P. R. Spackman, D. Jayatilaka, M. A. Spackman, The University of Western Australia, Australia, 2017.

[76] S. L. Tan, M. M. Jotani, E. R. T. Tiekink, Acta Crystallogr. Sect. E 75 (2019) 308-318.

[77] Y. J. Tan, Y. S. Tan, C. I. Yeo, J. Chew, E. R. T. Tiekink, J. Inorg. Biochem. 192 (2019) 107-118.

[78] M. E. Levison, Infect. Dis. Clin. North Am. 18 (2004) 451-465.

[79] B. R. Levin, F. Baquero, P. P. Ankomah, I. C. McCall, Trends Microbiol. 25 (2017) 878-892.

[80] J. Nemeth, G. Oesch, S. P. Kuster, J. Antimicrob. Chemother. 70 (2015) 382-395.

[81] L.H. Al-Wahaibi, N. Alvarez, O. Blacque, N. Veiga, A.A. Al-Mutairi, A.A. El-Emam, Molecules 25 (2020) 1934.

[82] S.K. Straus, R.E.W. Hancock, Biochim. Biophys. Acta 1758 (2006) 1215-1223.

[83] J.O. Adeyemi, D.C. Onwudiwe, A.C. Ekennia, R.C. Uwaoma, E.C. Hosten, Inorg. Chim. Acta 477 (2018) 148-159.

Table 1

Crystal data and refinement details for compounds **2**-**8**.

Compound	**2**	**3**	**4**	**5**	**6**
Formula	$C_{29}H_{30}O_2Sn$	$C_{52}H_{84}O_{10}Sn_4$	$C_{108}H_{132}O_{18}Sn_6$	$C_{15}H_{28}O_3Sn$	$C_{30}H_{32}O_2Sn$
Formula weight	529.22	1343.95	2430.26	375.06	543.24
Crystal colour	Colourless	Colourless	Colourless	Colourless	Colourless
Crystal size/mm^3	0.18 × 0.29 × 0.40	0.29 × 0.34 × 0.34	0.09 × 0.09 × 0.12	0.21 × 0.23 × 0.25	0.21 × 0.23 × 0.25
Crystal system	Triclinic	Triclinic	Triclinic	Monoclinic	Monoclinic
Space group	$P\bar{1}$	$P\bar{1}$	$P\bar{1}$	$P2_1/c$	$P2_1/c$
a/Å	10.6294(5)	10.7891(4)	10.9275(8)	6.7994(6)	11.8587(5)
b/Å	11.2196(6)	11.2192(4)	16.1173(9)	10.9676(10)	19.4239(8)
c/Å	11.2956(5)	12.7586(5)	16.4920(11)	22.657(3)	11.0727(4)
α/°	77.523(4)	97.827(3)	67.873(6)	90	90
β/°	72.559(4)	99.853(3)	76.821(6)	95.782(9)	97.887(4)
γ/°	79.975(4)	113.286(3)	75.605(6)	90	90
V/Å^3	1246.13(11)	1361.73(9)	2576.8(3)	1681.0(3)	2526.38(18)
Z	2	1	1	4	4
D_c/g cm^{-3}	1.410	1.639	1.566	1.482	1.428
F(000)	540	676	1224	768	1112
μ(Mo$K\alpha$)/mm^{-1}	1.048	1.866	1.497	1.522	1.035
Measured data	9105	10319	20708	6605	10007
θ range/°	3.2 – 28.7	3.3 – 28.7	2.9 – 28.8	3.3 – 29.1	3.6 – 29.0
Unique data	5561	6165	11632	3815	5759
Observed data ($I \geq 2.0\sigma(I)$)	4940	5340	8890	3332	4625
No. parameters	289	302	595	182	298
R, obs. data; all data	0.031; 0.083	0.023; 0.057	0.039; 0.077	0.038; 0.103	0.042; 0.082
a; b in weighting scheme	0.051; 0.367	0.031; 0.800	0.032; 0.841	0.061; 1.298	0.033; 0.590
R_w, obs. data; all data	0.037; 0.088	0.030; 0.062	0.062; 0.087	0.047; 0.107	0.058; 0.089
Range of residual electron density peaks/eÅ^{-3}	-0.43 – 0.75	-0.63 – 0.60	-0.65 – 1.05	1.70 – 1.05	-0.90 – 0.47

Compound	**7**	**8**
Formula	$C_{32}H_{52}O_4Sn$	$C_{38}H_{50}O_5Sn$
Formula weight	619.45	705.47
Crystal colour	Colourless	Colourless
Crystal size/mm^3	0.51 × 0.56 × 0.59	0.15 × 0.19 × 0.25
Crystal system	Monoclinic	Orthorhombic
Space group	*C*2/*c*	*Pccn*
a/Å	19.8489(17)	12.8110(6)
b/Å	7.1831(5)	19.3164(10)
c/Å	23.0559(16)	13.2171(5)
α/°	90	90
β/°	109.019(9)	90
γ/°	90	90
V/Å^3	3107.8(4)	3270.7(3)
Z	4	4
D_c/g cm^{-3}	1.324	1.433
F(000)	1304	1468
μ(Mo*K*α)/mm^{-1}	0.855	0.824
Measured data	5936	8687
θ range/°	3.3 – 29.0	3.1 – 29.0
Unique data	3503	3795
Observed data ($I \geq 2.0\sigma(I)$)	3089	2775
No. parameters	169	203
R, obs. data; all data	0.044; 0.099	0.039; 0.082
a; *b* in weighting scheme	0.052; 0.602	0.038; 0.567
R_w, obs. data; all data	0.053; 0.104	0.060; 0.092
Range of residual electron density peaks/eÅ^{-3}	-0.65 – 0.52	-0.54 – 0.30

Table 2

Anti-bacterial activity of organotin compounds (**1**, **2**, **5**-**7**), precursors (**S1-S3)**, pro-ligands (**HL^1 and HL^2**) and standard anti-biotics (Tetracycline and Chloramphenicol) screened using the disc diffusion method. Each disc contained 30 µg of compound/anti-biotic.[a]

Bacterial species	1	2	5	6	7	S1	S2	S3	L1	L2	Tetracycline	Chloramphenicol
Gram-positive bacteria												
E. faecalis	-	16	-	10	10	-	16	16	-	-	30	30
S. pyogenes	-	18	-	11	11	-	20	18	-	-	26	29
S. epidermidis	-	18	-	13	13	-	19	18	-	-	30	30
S. aureus (MRSA)	-	17	7	8	8	-	18	14	-	-	27	24
E. faecium	-	17	-	-	-	-	14	11	-	-	27	24
L. monocytogenes	-	12	-	9	9	-	15	15	-	-	27	24
S. penumoniae	-	15	-	9	9	-	19	17	-	-	33	30
Gram-negative bacteria												
K. pneumoniae	-	-	-	-	-	-	8	14	-	-	24	26
K. quasipneumoniae	-	-	-	-	-	-	-	9	-	-	24	26
P. aeruginosa	-	-	-	-	-	-	-	-	-	-	10	11
S. enterica 8	-	-	-	-	-	-	-	10	-	-	16	25
E. coli ATCC 11775	-	-	-	-	-	-	-	9	-	-	20	25
E. coli K1	-	-	-	-	-	-	8	7	-	-	23	26
S. flexneri	-	7	-	-	10	-	7	12	-	-	25	29
P. vulgaris	-	-	-	10	-	-	7	10	-	-	9	17
V. parahaemolyticus	-	12	-	10	10	-	14	15	-	-	24	25

[a] A zone of inhibition was not detected. All experiments were performed in triplicate. The smallest zone of inhibition (mm) recorded in the three independent studies is presented in this Table.

Table 3

MIC (μg/mL) and MBC/MIC ratio for organotin compounds (**2**, **6** and **7**), precursors (**S2** and **S3**) and standard anti-biotics (Tetracycline and Chloramphenicol) against eight pathogenic bacteria[a-c]

Bacterial Species	**2**		**6**		**7**		**S2**		**S3**		**Tetracycline**		**Chloramphenicol**	
	MIC	MBC/MIC	MIC	MBC/MIC	MIC	MBC/MIC	MIC	MBC/MIC	MIC	MBC/MIC	MIC	MBC/MIC	MIC	MBC/MIC
E. faecalis	3.125	4	3.125	4	25	ND	0.78	8	3.125	ND	0.198	32	3.125	ND
E. faecium	1.56	16	3.125	8	50	ND	1.56	8	25	ND	0.198	253	6.25	ND
S. aureus (MRSA)	0.78	32	1.56	16	25	ND	0.78	16	6.25	ND	0.39	128	12.5	ND
S. epidermidis	0.78	16	0.78	16	12.5	8	0.78	16	1.56	16	0.198	2	3.125	8
S. pneumoniae	1.56	8	1.56	8	25	4	1.56	4	6.25	8	0.39	8	6.25	16
S. pyogenes	0.78	16	0.78	16	12.5	ND	0.78	16	3.125	8	0.198	4	3.125	4
S. flexneri	12.5	ND	12.5	ND	25	ND	6.25	ND	3.125	ND	1.56	32	1.56	ND
V. parahaemolyticus	1.56	4	3.125	2	25	2	0.78	8	3.125	4	0.39	128	0.78	64

[a] MIC-minimum inhibitory concentration (μg/mL); MBC: minimum bactericidal concentration (μg/mL); MBC/MIC ratio ≤ 4 indicates bactericidal activity; MBC/MIC ratio >4 indicates a bacteriostatic activity; ND – MBC/MIC could not be determined as bacterium had grown across all tested concentrations, with MBC >100 μg/mL.

[b] The presented MIC values are the lowest inhibitory concentrations obtained from three independent experiments conducted in triplicate.

[c] **HL^1** and **HL^2** did not show anti-bacterial activity as bacterial cells grew at all concentrations tested (0.78 – 100 μg/mL), hence data are not presented in the table.

Table 4

Summary of *in vitro* time-kill study of organotin compounds **2** and **6** on *S. pyogenes*, *S. epidermidis* and *S. Aureus* (MRSA).

Bacterial species	Complex	Log10 CFU/mL[a]														
		1/2 × MIC					1 × MIC					2 × MIC				
		1 h	2 h	4 h	8 h	24 h	1 h	2 h	4 h	8 h	24 h	1 h	2 h	4 h	8 h	24 h
S. pyogenes	**2**	0.08	0.02	0.25	0.59	4.89	-0.03	-0.04	0.13	0.27	1.71	0.04	-0.07	-0.04	-0.28	-0.83
	6	0.01	0.24	0.35	1.37	4.98	0.03	0.21	0.33	0.47	1.79	0.06	0.17	0.17	0.08	0.96
S. epidermidis	**2**	0.01	0.07	0.25	0.54	4.18	-0.01	-0.04	0.11	0.11	1.56	0.04	-0.02	0	-0.62	1.18
	6	-0.01	0.05	0.31	1.24	6.12	0.01	0.00	0.16	0.32	1.75	0.02	0.00	0.03	-0.027	1.84
S. Aureus (MRSA)	**2**	0.09	0.27	1.27	2.41	4.53	0.01	-0.01	-0.03	0.16	4.26	0.06	0.03	0.00	0.05	3.67

[a] Values are the mean of values obtained from three independent biological replicates, each biological replicate comprised three technical replicates; a negative value indicates a reduction in bacterial number whereas a positive value indicates an increase in the number of bacterial cells.

Table 5

Cytotoxicity of organotin compounds (**1**, **2** and **5**-**7**), precursors (**S1**-**S3)**, pro-ligands (**HL^1 and HL^2**) measured as $\log_{10}(CC_{50})$ on the normal human cell line, HEK293T[a]

Compounds	$\log_{10}[CC_{50} \pm SE]$ (µg/mL)	Controls	$\log_{10}[CC_{50} \pm SE]$ (µg/mL)
1	1.390 ± 0.148	**S1**	1.009 ± 0.114
2	0.079 ± 0.035	**S2**	-0.046 ± 0.028
5	1.579 ± 0.166	**S3**	-0.141 ± 0.064
6	0.084 ± 0.046	**HL^1**	>2
7	0.421 ± 0.045	**HL^2**	>2

[a] The $\log_{10}(CC_{50})$ (µg/mL) value indicates the cytotoxic concentration at which a compound is able to kill 50% the original human cell population seeded in a well of a 96-well plate.

Legends to Scheme and Figures

Scheme 1. Synthetic methodologies used for obtaining organotin(IV) compounds **1**-**9**. The numbers at the pro-ligands (HL^1 and HL^2) denote the atom-numbering protocol used for the NMR signal assignment.

Fig 1. The molecular structures of (a) $Ph_3Sn(L^1)$ **2** (25% probability level), (b) $\{[Me_2Sn(L^1)]_2O\}_2$ **3** (50% probability level) and (c) $[BzSn(O)(L^1)]_6$ **4** (25% probability level), showing the atom labelling schemes and anisotropic displacement parameters. The unlabelled atoms are related by the symmetry operation 2-x, 2-y, 2-z (**3**) and 2-x, 1-y, -z (**4**).

In **3**, the carbon atoms are indicated by numbers only to reduce cluttering. Selected geometric parameters for the bridging carboxylate ligands in **3**: Sn1–O4 = 2.141(3), Sn2–O5 = 2.140(3), C1–O4 = 1.260(5), C1–O5 = 1.252(5), Sn1–O6 = 2.167(3), Sn3–O7 = 2.139(3), C12–O6 = 1.257(5), C12–O7 = 1.266(5), Sn3–O8 = 2.140(3), Sn2–$O9^i$ = 2.138(3), C23–O8 = 1.264(5), C23–O9 = 1.259(4) Å.

Fig 2. The molecular structures of (a) $Me_3Sn(L^2)OH_2$ **5** (25% probability level), (b) $[Ph_3Sn(L^2)]_n$ **6** (25% probability level; the arrows indicate the links to generate the supramolecular, one-dimensional coordination polymer shown in (c)), (d) $Bu_2Sn(L^2)_2$ **7** (25% probability level) and (e) $Bz_2Sn(L^2)_2OH_2$ **8** (35% probability level), showing the atom labelling schemes and anisotropic displacement parameters. The unlabelled atoms are related by the symmetry operations 1-x, y, 1½-z (**7**) and 1½-x, ½-y, z (**8**).

Fig 3. Molecular packing sustained by hydrogen bonding in the crystals of **5** and **8**: (a) **5**, a view of the supramolecular layer in the *ab*-plane sustained by water-O–H···O(carboxylate) hydrogen bonding and (b) a view of the zig-zag supramolecular chain along the *c*-axis sustained water-O–H···O(carboxylate) hydrogen bonding. Non-participating hydrogen atoms have been omitted for reasons of clarity.

Geometric (Å, °) details of the intermolecular interactions:

5

A	H	B	A–H	H···B	A···B	A–H···B	Symmetry operation
O3	H1o	O2	0.82(3)	1.88(3)	2.699(4)	175(8)	-x, ½+y, ½-z
O3	H2o	O1	0.82(4)	1.99(4)	2.807(4)	176(3)	1-x, ½+y, ½-z

8

O3	H1o	O1	0.82(3)	2.14(3)	2.858(3)	147(3)	x, ½-y, -½+z

Fig 4. Time-kill curves for **2** against (a) *S. pyogenes*, (b) *S. epidermidis* and (c) *S. aureus* (MRSA). The bactericidal level is indicated by the dashed line - - -, negative control ●, ½ × MIC ▲, 1 × MIC ♦ and 2 × MIC ×.

Fig 5. Time-kill curves for **6** against (a) *S. pyogenes* and (b) *S. epidermidis*. The bactericidal level is indicated by the dashed line - - -, negative control ●, ½ × MIC ▲, 1 × MIC ♦ and 2 × MIC ×.